

This item is the archived peer-reviewed author-version of:

Lipid oxidation : role of membrane phase-separated domains

Reference:

Oliveira Maria Cecilia, Yusupov Maksudbek, Bogaerts Annemie, Cordeiro Rodrigo M.- Lipid oxidation : role of membrane phase-separated domains
Journal of Chemical Information and Modeling - ISSN 1549-9596 - 61:6(2021), p. 2857-2868
Full text (Publisher's DOI): <https://doi.org/10.1021/ACS.JCIM.1C00104>
To cite this reference: <https://hdl.handle.net/10067/1797660151162165141>

Lipid Oxidation: Role of Membrane Phase- Separated Domains

*Maria C. Oliveira^{†, ‡}, Maksudbek Yusupov[‡], Annemie Bogaerts[‡], Rodrigo M. Cordeiro^{† *}*

[†]Centro de Ciências Naturais e Humanas, Universidade Federal do ABC, Avenida dos Estados 5001, CEP 09210-580 Santo André, SP, Brazil

[‡]Research Group PLASMANT, Department of Chemistry, University of Antwerp, Universiteitsplein 1, B-2610 Antwerp, Belgium

ABSTRACT

Lipid oxidation is associated with several inflammatory and neurodegenerative diseases, but many questions to unravel its effects on biomembranes are still open due

1
2
3 to the complexity of the topic. For instance, recent studies indicated that phase-
4
5
6 separated domains can have a significant effect on membrane function. It is reported
7
8
9 that domain interfaces are “hot spots” for pore formation, but the underlying
10
11
12 mechanisms and the effect of oxidation-induced phase separation on membrane remain
13
14
15 elusive. Thus, to evaluate the permeability of the membrane coexisting of liquid-ordered
16
17
18 (Lo) and liquid-disordered (Ld) domains, we performed atomistic molecular dynamics
19
20
21 simulations. Specifically, we studied the membrane permeability of non-oxidized or
22
23
24 oxidized homogeneous membranes (single-phase), and at the Lo/Ld domain interfaces
25
26
27
28 of heterogeneous membranes, where the Ld domain is composed of either oxidized or
29
30
31 non-oxidized lipids. Our simulation results reveal that the addition of only 1.5% of lipid
32
33
34 aldehyde molecules at the Lo/Ld domain interfaces of heterogeneous membranes
35
36
37 increases the membrane permeability, whereas their addition at homogeneous
38
39
40 membranes does not have any effect. This study is of interest for a better understanding
41
42
43 of cancer treatment methods based on oxidative stress (causing among others lipid
44
45
46 oxidation), such as plasma medicine and photodynamic therapy.
47
48
49
50
51
52
53
54
55
56
57
58
59
60

INTRODUCTION

The major structural lipids in eukaryotic membranes are the phospholipids. They have a nearly cylindrical molecular geometry composed of saturated and cis-unsaturated fatty acid chains, which render them fluid at room temperature.¹ These fatty acid chains can be oxidized by specific enzymes² or free radicals, namely reactive oxygen and nitrogen species (RONS)³. The oxidative attack by free radicals may lead to oxidative stress situations in the fatty acid chains, generating relatively stable products bearing functional groups, such as hydroperoxide, hydroxyl and truncated acyl chains with aldehyde and carboxylic groups.^{4,5} These oxidized lipids affect the microscopic and macroscopic properties of the membrane, which may be associated with several inflammatory, cancer and neurodegenerative diseases.^{6,7,8}

Lipids and proteins can diffuse laterally in the membrane, creating a random mosaic-like structure that has the fluidity of vegetable oil.⁹ Despite the latter, there is a large body of experimental evidence suggesting that, rather than being randomly

1
2
3 distributed, lipids and proteins are able to organize in nanodomains, enriched in
4
5
6
7 cholesterol and saturated sphingolipids, revealing a lipid heterogeneity in the
8
9
10 membrane.^{10,11} These domains are referred to as “lipid rafts” and serve as rafts for the
11
12
13
14 transport of selected molecules¹² or as relay stations in intracellular signaling.^{13,14}
15
16
17 Changes in raft sizes can affect the function of the plasma membrane, for example, by
18
19
20 altering the capacity of membrane domains to accommodate proteins that must interact
21
22
23
24 for signaling. Several experimental works have demonstrated the heterogeneity in
25
26
27
28 biomembranes.^{15,16,17} However, there are many technical challenges associated with
29
30
31 the observation of nanometer-scale changes in lipid composition.^{18,19}
32
33
34
35

36 The surface of any living cell, either prokaryotic or eukaryotic, is a complex
37
38
39 assembly of a variety of molecular components comprising lipids and embedded
40
41
42
43 proteins. It is supported by the cytoskeletal meshwork attached to the plasma
44
45
46
47 membrane via anchoring proteins. Arumugam and co-workers demonstrated that the
48
49
50 interaction of transmembrane or membrane binding proteins with the cytoskeleton
51
52
53
54
55
56
57
58
59
60

1
2
3 maintains the heterogeneity (phase separation) of the plasma membrane, even above
4
5
6
7 the transition temperature.²⁰
8
9

10
11 Lipid rafts form distinct liquid-ordered (Lo) phase-separated domains in the lipid
12
13 bilayer, dispersed in a liquid-disordered (Ld) matrix of unsaturated lipids, which might
14
15 play a significant role in the plasma membrane of living cells.^{21,22} In addition, lipid
16
17 oxidation may induce Lo/Ld phase separation in membranes.²³ Tsubone and co-
18
19 workers proposed that the lipid hydroperoxide, an oxidized lipid with cylindrical
20
21 molecular geometry,²⁴ is a promoter of Lo/Ld phase separation, whereas the lipid
22
23 carboxylic acid, which has a conical molecular geometry, does not cause phase
24
25 separation, but directly influences the bilayer deformation and membrane leakage.²⁵
26
27
28
29 Thus, oxidation-induced phase separation might have serious consequences for cell
30
31 membranes that are subject to oxidative stress.
32
33
34
35
36
37
38
39
40
41
42
43
44
45
46

47 The fluidity of a lipid bilayer is affected by the hydration level, temperature, lipid
48
49 composition, and cholesterol content of the membrane. At low temperature, the lipid
50
51 tails can pack closely together to form a crystalline lamellar subgel phase (Lc), with
52
53
54
55
56
57
58
59
60

1
2
3 hydrocarbon chains untilted with respect to the bilayer normal, and the long axis of the
4
5
6
7 headgroup oriented parallel to the bilayer normal. Upon heating, the L_c phase
8
9
10 undergoes a sub-transition to a lamellar gel phase less ordered than the L_c phase, with
11
12
13 untilted chains (L_β) (fairly rigid) or tilted chains (L_β') (less rigid). Addition of cholesterol
14
15
16 transforms the gel phase into a L_o phase. At higher temperatures, i.e., during the so-
17
18 called pre-transition, an interconversion between two different gel phases takes place:
19
20
21 the L_β' phase transforms into a periodic modulation called the rippled gel phase (P_β').
22
23
24 Upon further heating, the P_β' phase undergoes a highly cooperative transition to a
25
26
27 lamellar liquid crystalline phase (L_α) that is more fluid^{26,27} (Figure 1).
28
29
30
31
32
33
34
35

36 Phase-separated domains (caused by lipid rafts) are very important in membrane
37
38
39 research. Theoretical studies suggested that the interfaces between phase-separated
40
41
42 domains are regions where pore formation is facilitated. The interface region was
43
44
45 roughly 2–4 orders of magnitude more permeable to Na⁺ ions than the fluid phase.²⁸
46
47
48
49 However, for the membrane as a whole to be leaky, it needs to be strongly
50
51
52
53 microheterogeneous with a large number of interfacial regions. That is why membranes
54
55
56
57
58
59
60

1
2
3 become leaky near the gel-fluid transition temperature: many interfacial regions develop
4
5
6
7 since the quasi-critical transition regime is approached.^{29,30,31} Ghysels and co-workers
8
9
10 studied the permeation of oxygen and water molecules through membranes with Lo and
11
12
13 Ld phases using molecular dynamics (MD) simulations and electron paramagnetic
14
15
16 resonance (EPR) spectroscopy. They demonstrated that the oxygen and water
17
18
19 molecules enter through the Lo phase, diffuse laterally in the membrane core, and then
20
21
22
23 leave the membrane along the boundary regions.³² Nevertheless, the interfacial
24
25
26
27 permeability is still not fully understood, being a challenge both experimentally and in
28
29
30
31 computer simulations.
32
33
34
35
36
37
38
39
40
41
42
43
44
45
46
47
48
49
50
51
52
53
54
55
56
57
58
59
60

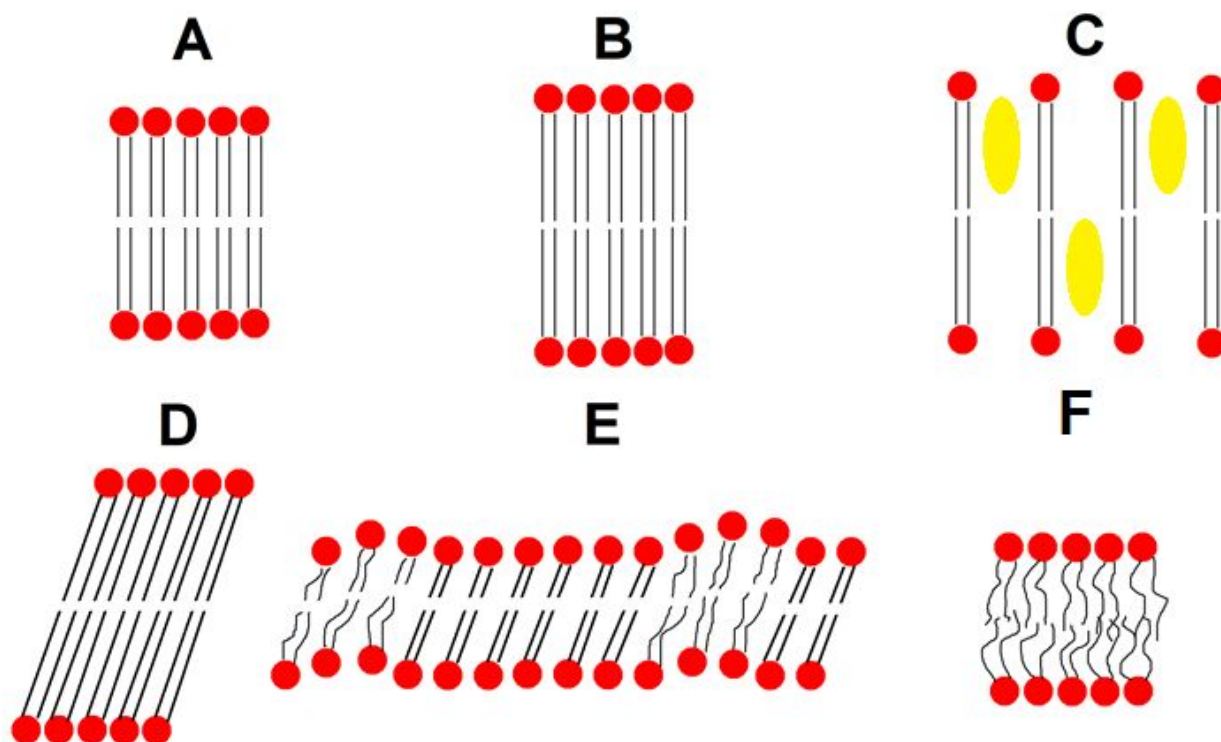


Figure 1. Schematic representation of the various lamellar lipid phases: (A) crystalline lamellar subgel (L_c); (B) gel with untilted chains (L_β); (C) liquid-ordered (L_o), where the filled oval circles in yellow represent cholesterol molecules; (D) gel with tilted chains (L_β'); (E) rippled gel (P_β') and (F) liquid crystalline (L_α).

It is well known that lipid oxidation products affect the microscopic and macroscopic properties of the membrane, inducing structural and conformational

1
2
3 changes related to the area per lipid, lipid order, bilayer thickness,³³ and bilayer
4
5
6
7 hydration profile.³⁴ These changes might in turn induce pore formation and thus affect
8
9
10 the membrane permeability. Recently, we showed that nitrated lipids (also produced by
11
12
13 free radicals) considerably increase the membrane permeability.³⁵ Boonnoy and co-
14
15
16
17 workers observed the formation of water defects induced by both lipid aldehydes and
18
19
20 lipid hydroperoxides, where full pore formation was observed only in the bilayer
21
22
23 consisting of lipid aldehydes. At 50% oxidation with lipid aldehydes, the pores were
24
25
26
27 stable. However, at higher concentrations, the pores became unstable and micellation
28
29
30
31 occurred within 1 μ s.³⁶
32
33
34
35

36 Van der Paal and co-workers showed that the membrane permeability may be
37
38
39 influenced by different lipid molecules present in the membrane. For instance, the
40
41
42 presence of both aldehyde fragments (produced as a result of lipid chain break) and
43
44
45 cholesterol were shown to reduce the susceptibility of membranes to pore formation.³⁷
46
47
48
49 Thus, it can be expected that other oxidized lipids formed in the membrane may
50
51
52
53 modulate the permeabilization effect of lipid aldehydes. In this study, we investigate the
54
55
56
57
58
59
60

1
2
3 role of lipid oxidation on the permeability of phase-separated domains, using MD
4
5
6
7 simulations. We hope that our study contributes to a better understanding of the effects
8
9
10 of products generated during photosensitized reactions used in photodynamic
11
12
13 therapies,³⁸ as well as during lipid oxidation caused by plasma medicine.^{39,40}
14
15
16
17

18 METHODS

19
20
21
22

23 We performed MD simulations using the software GROMACS version 5.1.2,⁴¹
24
25 applying the united-atom GROMOS 53A6 force field.⁴² We used well-validated models
26
27 for the description of unsaturated lipids⁴³ and lipid hydroperoxides.⁴⁴ We adopted
28
29 interatomic interaction parameters for the aldehyde functional groups from the standard
30
31 GROMOS 53A6 force field library.^{42,45} This force field reproduces very well experimental
32
33 data from biomolecules in general,⁴⁶ and specifically from biomembranes.⁴³
34
35
36
37
38
39
40
41
42
43
44

45 In our simulations, we used heterogeneous model membranes composed of
46
47 POPC (1-palmitoyl-2-oleoyl-sn-glycero-3-phosphocholine) molecules and their oxidation
48
49 products that contain hydroperoxide (POPCOOH) and aldehyde (POPC-ALD) functional
50
51 groups. The hydroperoxide group was added with R stereocenter at C9 carbon (see
52
53
54
55
56
57
58
59
60

Figure 2). All initial systems were built using the Packmol software,⁴⁷ and graphical renderings were produced using the VMD software version 1.9.3.⁴⁸

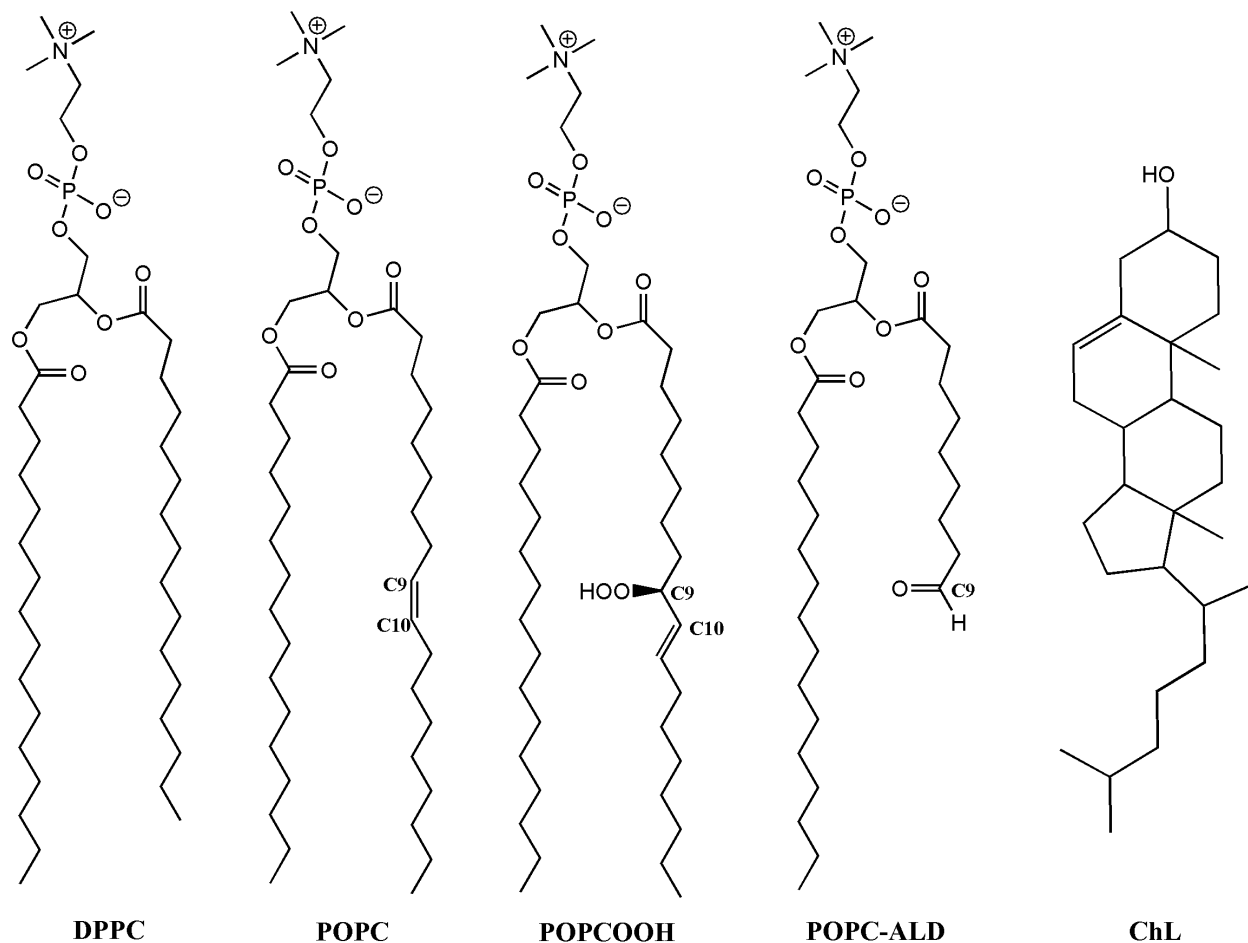


Figure 2. Structure of each lipid and cholesterol (ChL) used in our simulations. See text for the full names.

MD Protocol

We started the simulations from a membrane with pre-formed domains with assumed compositions, consistent with either the Lo or Ld phases. Each system was composed of coexisting Lo and Ld domains: one consisting of DPPC (1,2-dipalmitoyl-phosphatidylcholine) + cholesterol (ChL) molecules (Lo phase), and another consisting of native POPC or POPCOOH (Ld phase). Earlier simulations have suggested the formation of a constriction region (i.e., a region with minimal membrane thickness) at the gel/fluid interface, which could also enhance membrane permeability.²⁸ Thus, we added POPC-ALD lipid molecules to the Lo/Ld domain interface region of our model membranes, because it is the region where they might elicit the strongest effect. These systems were then covered with water molecules on top and at the bottom. The structure of each lipid, as well as cholesterol, used in our simulations can be seen in Figure 2. They are representative of typical products of lipid oxidation.^{3,49}

Water molecules were modeled with the simple point charge (SPC) model.⁵⁰ Periodic boundary conditions were used in all Cartesian directions. Newton's equations

1
2
3 of motion were integrated using the leap-frog algorithm with a time step of 2 fs. A cut-off
4
5
6 radius of 1.4 nm was used for non-bonded (Lennard-Jones) interactions. Coulomb
7
8
9
10 interactions were treated using the PME method. The covalent bond lengths were
11
12
13
14 constrained using the LINCS algorithm.
15
16
17

18 We performed a steepest descent energy minimization, followed by equilibration
19
20
21 at the NPT ensemble for at least 300 ns. The temperature was maintained close to the
22
23
24 physiological temperature (310 K) by coupling the system to an external temperature
25
26
27 bath using the Nose-Hoover thermostat.^{51,52} The temperature coupling constant was 0.5
28
29
30
31 ps. The pressure was also maintained at around 1 bar by coupling the system to an
32
33
34 external pressure bath using the Parrinello-Rahman barostat.⁵³ The pressure coupling
35
36
37 was applied semi-isotropically with a coupling constant of 2 ps, and isothermal
38
39
40 compressibility of $4.5 \times 10^{-5} \text{ bar}^{-1}$.⁵⁴ Note that the chosen equilibration time (300 ns)
41
42
43
44 was sufficient, as the membrane areas of all systems converged within this time (see
45
46
47
48
49
50 Figure S1 in the Supporting Information (SI)).
51
52
53

54 Data Analysis

55
56
57
58
59
60

1
2
3 All membrane properties were calculated from the last 100 ns of the simulation.
4
5

6
7 The area per lipid of each domain was calculated by Voronoi tessellations implemented
8
9
10 in the voro++ software.⁵⁵ The area per lipid was calculated using a set of key atoms in
11
12
13 the Voronoi analysis. For lipids, both carbonyl carbons and the CH₁ group in the
14
15
16 glycerol moiety were used as key atoms. For cholesterol, the oxygen atom of the
17
18
19 hydroxyl group was used. The bilayer thickness was calculated using the gmx traj tool
20
21
22 of the GROMACS program. It was defined as the average distance along the z-axis
23
24
25 between the center of mass of the phosphorus atoms of both leaflets. The uncertainties
26
27
28 were calculated by standard deviation of the average values.
29
30
31
32
33
34
35

36 The distribution of the curvature order parameter was calculated using the
37
38
39 s_order program of the software Surface Assessment via Grid Evaluation (SuAVE),⁵⁶
40
41
42 with a mesh resolution of 40401 and corresponding bin values of 200. This program
43
44
45 calculates the average curvature order parameter distribution $P(\theta)$ of the angles θ
46
47
48 between the z-axis and the normal vectors of the surface rectangular grid partitions,
49
50
51 over all trajectory frames:
52
53
54
55
56
57
58
59
60

$$P(\theta) = \frac{1}{2}(3\cos^2(\theta) - 1) \quad (1)$$

The curvature order parameter ranges from $P(90^\circ) = -0.5$ to $P(0^\circ) = 1$. In the first case, the normal vector of the surface is perpendicular to the z -axis (larger curvatures). In the second case, the normal vector of the surface is parallel (smaller curvatures). The software for calculation of the number of water molecules crossing the membrane was developed by the research group of Prof. Alexandre Suman de Araujo, from IBILCE/UNESP.⁵⁷ The numbers of permeation events were calculated using a single model membrane, except for the POPCOOH + 6 POPC-ALD and DPPC + ChL / POPCOOH + 6 POPC-ALD, where 3 replicates were used for averaging.

RESULTS AND DISCUSSION

We performed MD simulations for model membranes composed of two coexisting domains: the Lo domain was composed of DPPC + ChL molecules and the Ld domain was composed of either POPC or POPCOOH lipids. We also performed MD simulations by adding different quantities of POPC-ALD lipid molecules to the Lo/Ld domain

interface regions of the membranes. The compositions of our model systems are given in Table 1 (and see also Figures 3 and 4).

Table 1. Composition of each simulated membrane. The number of POPC and oxidized lipids correspond to the total lipids in the two membrane domains.

| System | Number of molecules | | | | | Water | Box dimensions (nm) |
|-----------------------------------|---------------------|---------------|------|-----------------|----------|-------|---------------------|
| | ChL | native lipids | | oxidized lipids | | | |
| | | DPPC | POPC | POPCOOH | POPC-ALD | | |
| DPPC + ChL / POPC | 54 | 128 | 256 | – | – | 17524 | 18.74, 6.30, 8.75 |
| DPPC + ChL / POPC + 6 POPC-ALD | 54 | 128 | 244 | – | 12 | 17523 | 19.26, 6.09, 8.81 |
| DPPC + ChL / POPC | 54 | 128 | 192 | – | 64 | 17523 | 19.26, 6.09, 8.81 |

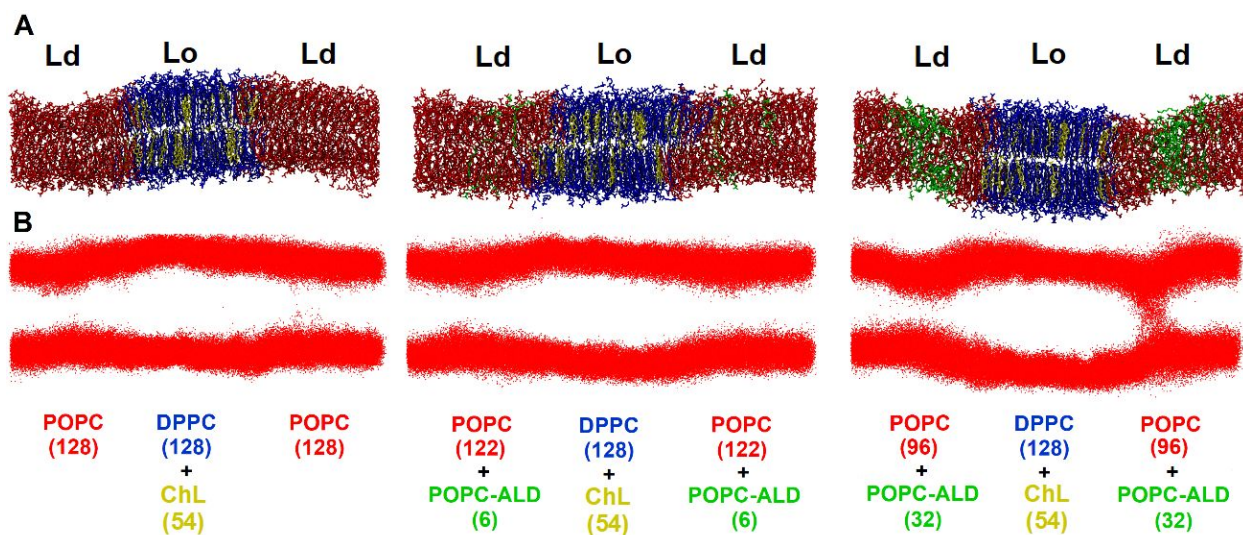
| | | | | | | | |
|--|----|-----|---|-----|----|-------|-------------------|
| + 32 POPC-ALD | | | | | | | |
| DPPC + ChL / POPCOOH | 54 | 128 | – | 256 | – | 17524 | 19.58, 6.35, 8.34 |
| DPPC+ ChL / POPCOOH + 6 POPC-ALD | 54 | 128 | – | 244 | 12 | 17524 | 23.64, 5.69, 7.69 |
| DPPC + ChL / POPCOOH + 16 POPC-ALD | 54 | 128 | – | 224 | 32 | 17524 | 21.04, 6.08, 8.11 |
| DPPC + ChL / POPCOOH + 32 POPC-ALD | 54 | 128 | – | 192 | 64 | 17523 | 19.83, 6.06, 8.52 |

Membrane Structural Properties

Note that our simulations reveal a thickness mismatch between different phases, i.e., the thickness of the Lo domain was larger than that of the Ld domain (Figure 3A and 4A). In line with previous studies of the gel/fluid coexistence,²⁸ the thickness did not decrease monotonically from the Lo to the Ld phase. Instead, a thickness minimum (i.e.,

1
2
3 a constriction region) is formed at the Lo/Ld interface (Figure 5), due to the elastic
4
5
6
7 deformation of the Ld domain in the region near to the domain interface.
8
9

10
11 By adding POPC-ALD lipid molecules at the Lo/Ld domain interfaces, we
12
13
14
15 observed more water molecules crossing the membrane through this region. The effect
16
17
18 was more pronounced in the POPC (Figure 3B) than in the POPCOOH domain (Figure
19
20
21
22 4B). We witnessed stronger undulations and membrane bending in the case of
23
24
25 POPCOOH (cf. Figures 3A and 4A), which can be the reason of the lower permeability
26
27
28 of the POPCOOH domain. For DPPC + ChL / POPCOOH + 16 POPC-ALD system, the
29
30
31
32 permeation was similar to DPPC + ChL / POPCOOH + 6 POPC-ALD system. Note that
33
34
35
36 the increase in the membrane permeability is more visible when we have a lot of POPC-
37
38
39 ALD molecules at the Lo/Ld domain interfaces. In order to determine the effect caused
40
41
42
43 by few POPC-ALD molecules, we will calculate the number of water molecules crossing
44
45
46 the membrane (see Section membrane permeability). Note that the Lo/Ld domain
47
48
49
50 interface region consists of a constriction region together with the gel/fluid interface (see
51
52
53 red rectangle in Figure S2).
54
55
56
57
58
59
60



23 **Figure 3. (A)** Snapshots of heterogeneous membranes at 300 ns of simulation, where
24
25
26 the Ld phase is composed of POPC lipid molecules. **(B)** Trajectories of water
27
28
29 molecules. Lipid molecules were removed for clarity and water molecules are
30
31
32 represented as red points. All frames of the last 100 ns were overlaid in order to
33
34
35
36
37 highlight the permeation path of water molecules.
38
39
40
41
42
43
44
45
46
47
48
49
50
51
52
53
54
55
56
57
58
59
60

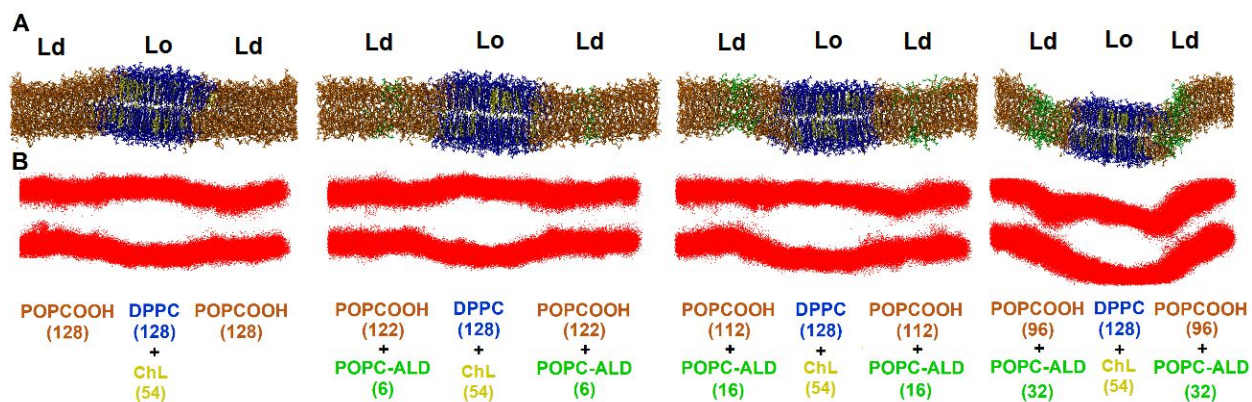


Figure 4. (A) Snapshots of heterogeneous membranes at 300 ns of simulation, where the Ld phase is composed of POPCOOH lipid molecules. (B) Trajectories of water molecules. Lipid molecules were removed for clarity and water molecules are represented as red points. All frames of the last 100 ns were overlaid in order to highlight the permeation path of water molecules.

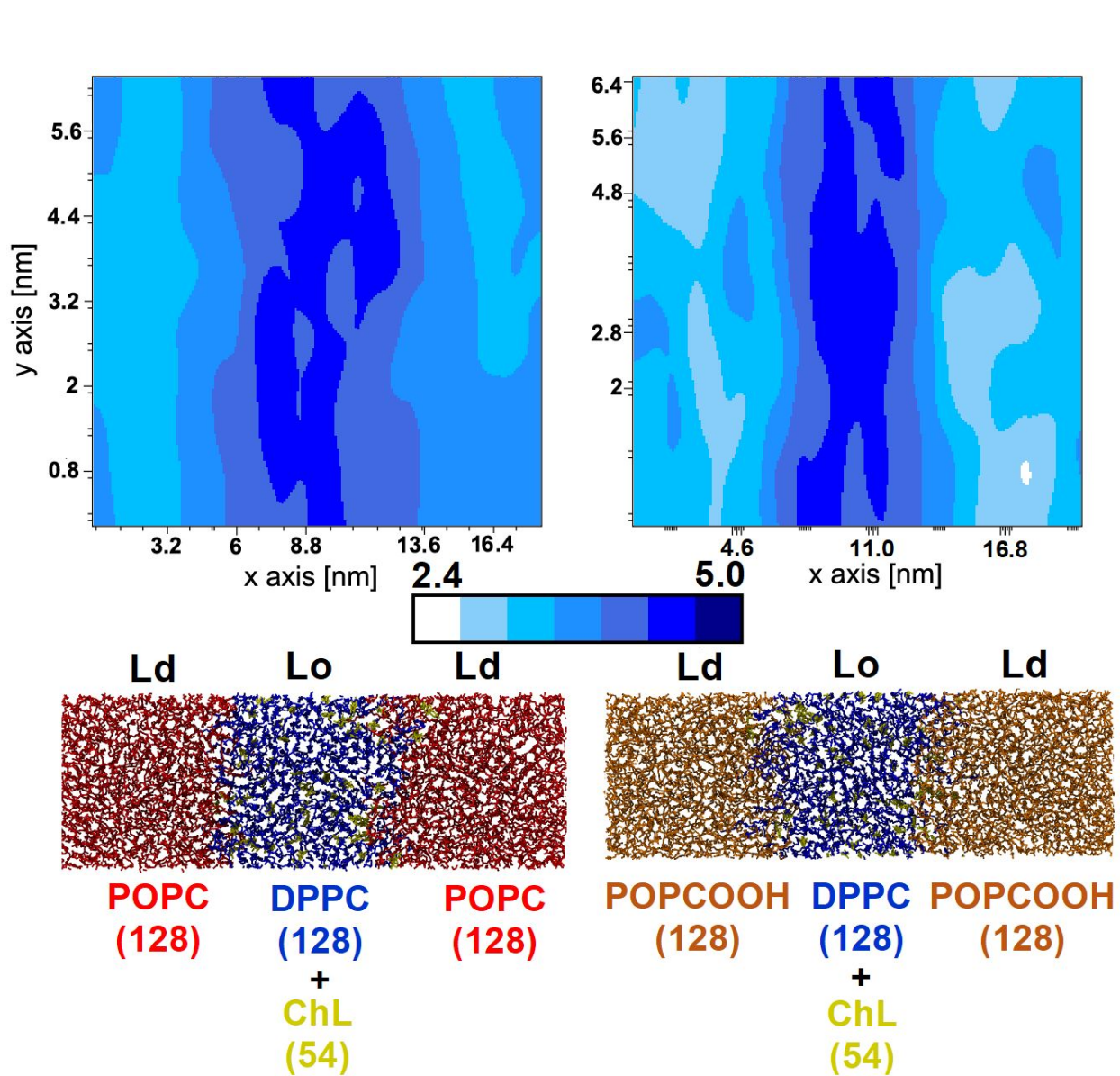


Figure 5. Two-dimensional frame-averaged distribution of the bilayer thickness calculated from the last 100 ns of simulation. The mesh resolution is 40401 and corresponding bin values are equal to 200. These distributions were calculated using the software SuAVE. Both panels represent a top view of the membrane systems. In the upper panel we can see the bilayer thickness of the bottom panel. Box sizes in x and y-

1
2
3 axes are the same in upper and bottom figures, but they are represented in different
4
5
6
7 scales.
8
9

10
11
12
13
14
15
16 Experimental measurements from literature revealed a 10-fold increase in
17
18
19 membrane permeability upon addition of minute amounts (2.5%) of lipid aldehydes.⁵⁸
20
21
22
23 However, molecular simulations showed the formation of membrane poration (which is
24
25
26 a measure for membrane permeability) only at aldehyde molar fractions larger than
27
28
29 50%.³⁶ We conjectured that: i) depending on composition or external effects such as
30
31
32
33 oxidation, membranes might become microheterogeneous at the nanoscopic scale; ii)
34
35
36 short-chain aldehydes that are formed along other oxidation products might have a
37
38
39 preference for the constriction region at the domain boundaries, where they would
40
41
42
43 concentrate and elicit a stronger permeabilization effect. Lipid lateral diffusion involves
44
45
46 time scales that are difficult to achieve in atomistic simulations. Many studies of the
47
48
49
50 membrane phase behavior were conducted with lower-resolution coarse-grained
51
52
53 models.^{59,60} Here, we pursued a simplified, yet meaningful strategy in which we
54
55
56
57
58
59
60

1
2
3
4 assumed an enhanced aldehyde concentration at the interface, and checked whether it
5
6
7 would contribute to membrane permeabilization.
8
9

10 11 **Area per Lipid and Bilayer Thickness** 12

13
14
15
16 Table 2 show the areas per lipid and membrane thicknesses recorded for all
17
18
19 studied systems. When no POPC-ALD lipid molecules were included, the area per lipid
20
21
22 of the POPC domain was $0.58 \pm 0.19 \text{ nm}^2$. Within the uncertainty this compares well
23
24
25 with the experimental values of 0.64 ± 0.01 and $0.67 \pm 0.01 \text{ nm}^2$ obtained for native
26
27
28 POPC at 303 and 323 K, respectively, from X-ray scattering.⁶¹ In the case of the
29
30
31 POPCOOH domain, the area per lipid was found to be $0.62 \pm 0.23 \text{ nm}^2$, hence around
32
33
34 7% higher than that of POPC. The average increase in area per lipid of the POPC
35
36
37 system with complete peroxidation was also found in the literature.⁶² An increase of the
38
39
40 area per lipid reflects the well-known effect of migration of $-\text{OOH}$ groups towards the
41
42
43 membrane surface.^{63,64} The area per DPPC at the L_o domain was $0.59 \pm 0.19 \text{ nm}^2$ in
44
45
46 the DPPC + ChL / POPC system, and $0.64 \pm 0.24 \text{ nm}^2$ in the DPPC + ChL / POPCOOH
47
48
49 system. The area per ChL in the DPPC + ChL / POPC system was $0.18 \pm 0.06 \text{ nm}^2$,
50
51
52
53
54
55
56
57
58
59
60

1
2
3
4 whereas it was $0.21 \pm 0.08 \text{ nm}^2$ in the DPPC + ChL / POPCOOH system (see Table 2).
5
6

7 The bilayer thickness of each domain reveals how much the Ld domain is thinner when
8
9
10 compared with the Lo domain (a thickness mismatch). Moreover, the Ld domain is
11
12
13 thinner when it is composed of oxidized lipids (see Table 2).
14
15
16
17

18 As is clear from Table 2, we obtained relatively large uncertainties in our
19
20
21 simulation data. This is due to the fact that the sampling of average values cannot
22
23
24 distinguish between lipids at the bulk of the domain and at the interface regions. One of
25
26
27 the evidences for this is that the area per lipid of homogeneous membranes (Table S1)
28
29 had much smaller uncertainties associated. It is in principle possible to calculate the
30
31
32 area per lipid locally, but we believe this has limited added value as the results would
33
34
35 also be strongly influenced by the strong curvature and undulations at the interfacial
36
37
38 region (Figure 4). On the qualitative level, the oxidized systems appeared to have
39
40
41 consistently higher values of area per lipid, as expected (Table 2). All model
42
43
44 membranes were simulated just a single time, except for the DPPC + ChL / POPCOOH
45
46
47 + 6 POPC-ALD system. The latter was simulated in triplicate in order to check for the
48
49
50
51
52
53
54
55
56
57
58
59
60

1
2
3 reproducibility of the results, and all structural properties of the membrane remained
4
5
6
7 equal within the uncertainties (Table S1).
8
9
10
11
12
13
14
15
16
17
18
19
20
21
22
23
24
25
26
27
28

29 **Table 2.** Area per lipid and bilayer thickness of all model membranes simulated. The
30
31 bilayer thickness is represented between brackets.
32
33
34
35
36

| System | Area per lipid (nm ²) and Bilayer thickness (nm) | | | | |
|-------------------|--|---------------|-----------|-----------------|----------|
| | ChL | native lipids | | oxidized lipids | |
| | | DPPC | POPC | POPCOOH | POPC-ALD |
| DPPC + ChL / POPC | 0.18±0.06 | 0.59±0.19 | 0.58±0.19 | – | – |

| | | | | | |
|---|-----------|-------------|-------------|-------------|-------------|
| | – | (4.54±0.03) | (3.81±0.03) | – | – |
| DPPC + ChL / POPC + 6 POPC-ALD | 0.20±0.06 | 0.59±0.19 | 0.58±0.19 | – | 0.60±0.19 |
| | – | (4.44±0.07) | (3.83±0.06) | – | (3.61±0.16) |
| DPPC + ChL / POPC + 32 POPC-ALD | 0.20±0.07 | 0.59±0.19 | 0.58±0.22 | – | 0.59±0.20 |
| | – | (4.52±0.04) | (3.70±0.04) | – | (2.97±0.09) |
| DPPC + ChL / POPCOOH | 0.21±0.08 | 0.64±0.24 | – | 0.62±0.23 | – |
| | – | (4.36±0.04) | – | (3.43±0.03) | – |
| DPPC+ ChL / POPCOOH + 6 POPC-ALD | 0.22±0.08 | 0.66±0.26 | – | 0.66±0.26 | 0.71±0.28 |
| | – | (4.47±0.03) | – | (3.22±0.03) | (3.03±0.13) |
| DPPC + ChL / POPCOOH + 16 POPC-ALD | 0.22±0.09 | 0.65±0.25 | – | 0.62±0.26 | 0.63±0.26 |
| | – | (4.37±0.04) | – | (3.32±0.03) | (3.29±0.09) |
| DPPC + ChL / POPCOOH + 32 POPC-ALD | 0.20±0.13 | 0.59±0.49 | – | 0.60±0.42 | 0.61±0.60 |
| | – | (4.32±0.11) | – | (3.50±0.09) | (3.10±0.07) |

1
2
3
4 We also calculated the surface curvature order parameter, represented in Figure
5
6
7 6 as two-dimensional frame-averaged distribution. It can help to pinpoint the local
8
9
10 positions where the membrane curvature changes, which can be visually correlated to
11
12
13 the presence of POPC-ALD lipid molecules. A positive (or negative) curvature order
14
15
16 parameter means that the membrane presents less (or more) bending.⁶⁵ The number of
17
18
19 POPC-ALD lipids placed at the domain interfaces is directly related to membrane
20
21
22 bending. We can also demonstrate this relation by calculating the Pearson correlation
23
24
25 coefficient (r) of the curvature order parameter vs position of POPC-ALD lipids (Figure
26
27
28 6). The Pearson correlation coefficient is a measurement of the strength and
29
30
31 association between two variables, i.e., it calculates the effect of changing one variable
32
33
34 on the changes in the other variable. The formula of the Pearson correlation coefficient
35
36
37 shows the relationship between the variables x and y , and yields values between -1 and
38
39
40
41
42
43
44
45 1:

$$r = \frac{N \sum xy - [(\sum x)(\sum y)]}{\sqrt{[N \sum x^2 - (\sum x)^2][N \sum y^2 - (\sum y)^2]}} \quad (2)$$

1
2
3 where N is the number of points.
4
5
6
7

8 According to Figure 6, we can see a large degree of association between the
9
10 curvature order parameter and the position of POPC-ALD lipids, with a positive linear
11
12 relationship, i.e., when the curvature order parameter increases, the position of POPC-
13
14 ALD lipids also increases. Therefore, the local membrane curvature increases upon
15
16 adding of POPC-ALD. The membrane surface was concave at the interface, forming an
17
18 interfacial constriction region with lower thickness. A similar feature has been identified
19
20 in literature at the gel/fluid interface of membranes, and it has been shown to lead to a
21
22 higher tendency for pore formation.²⁸
23
24
25
26
27
28
29
30
31
32
33
34
35
36
37
38
39
40
41
42
43
44
45
46
47
48
49
50
51
52
53
54
55
56
57
58
59
60

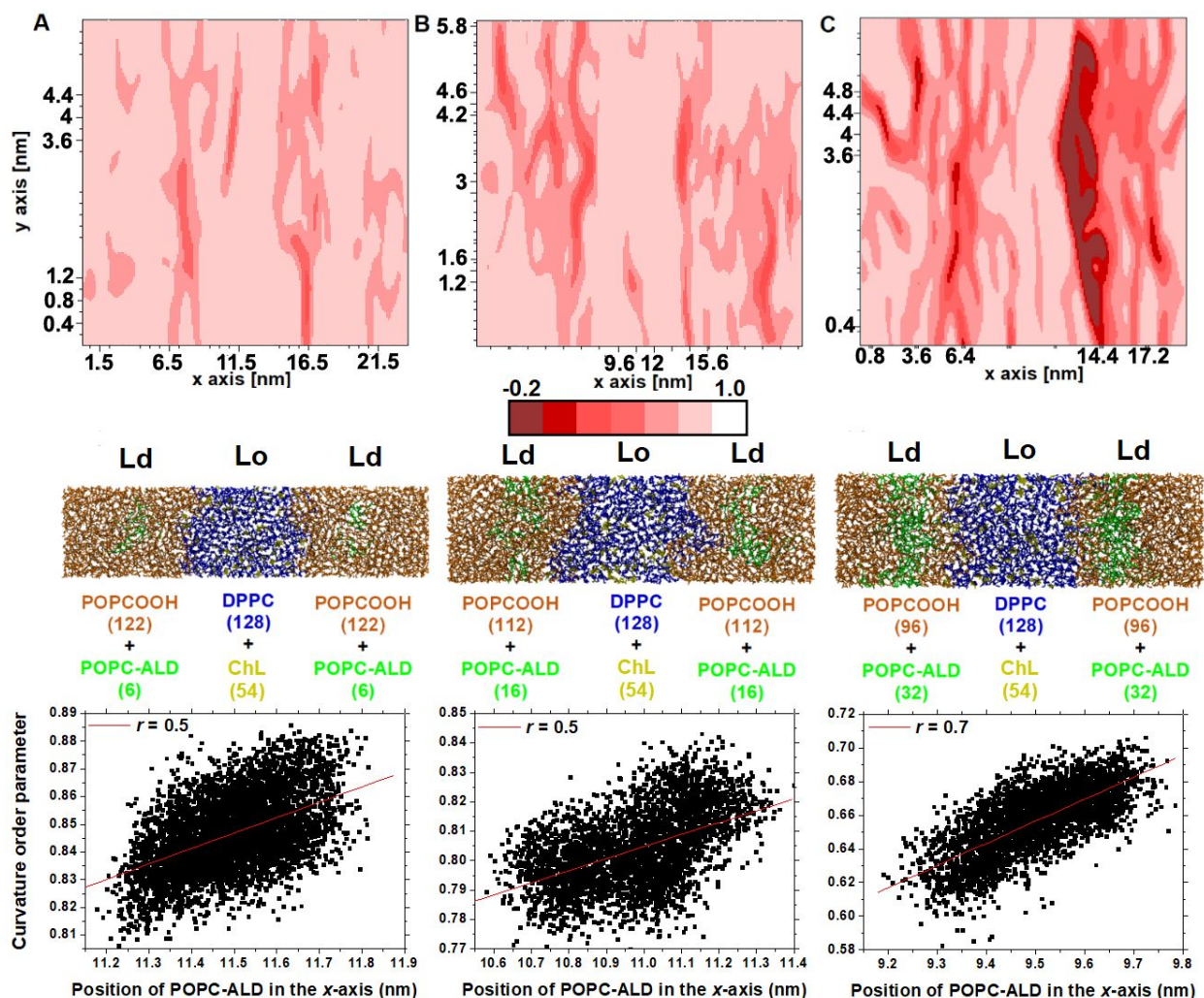


Figure 6. Two-dimensional frame-averaged distribution of the curvature order parameter calculated from the last 100 ns of simulation, for the different systems. These distributions were calculated using the software SuAVE. Both panels represent a top view of the membrane systems. In the upper panel we can see the membrane curvature of the bottom panel. It should be noted that the upper graphs and bottom snapshots are

1
2
3 not in the same scale. The bottom-most graphs represent the Pearson correlation
4
5
6
7 coefficient (r) of the curvature order parameter *vs* position of POPC-ALD lipids.
8
9

10
11
12
13
14
15
16 In addition, we calculated the average bilayer thickness (Figures 5, and Table 2).
17
18
19 The bilayer thickness of the POPC domain was 3.81 ± 0.03 nm, whereas for the
20
21
22 POPCOOH domain it was 3.43 ± 0.03 nm (Table 2), i.e., around 11% lower than for the
23
24
25 POPC domain. Because of the thinner bilayer, the POPCOOH domain became more
26
27
28 susceptible to membrane fluctuations. The cholesterol molecules largely help to
29
30
31 maintain the L_0 phase of the DPPC domain: the L_0 phase is thicker than the L_d phase
32
33
34 (Figure 5). The bilayer thickness of the L_0 domain was similar for both systems: $4.54 \pm$
35
36
37 0.03 and 4.36 ± 0.04 nm in the DPPC + ChL / POPC and DPPC + ChL/POPCOOH
38
39
40 systems, respectively (see Table 2). The values of the thickness mismatch between
41
42
43
44 different domains is displayed in Table S2.
45
46
47
48
49
50

51 Membrane Permeability

52
53
54
55
56
57
58
59
60

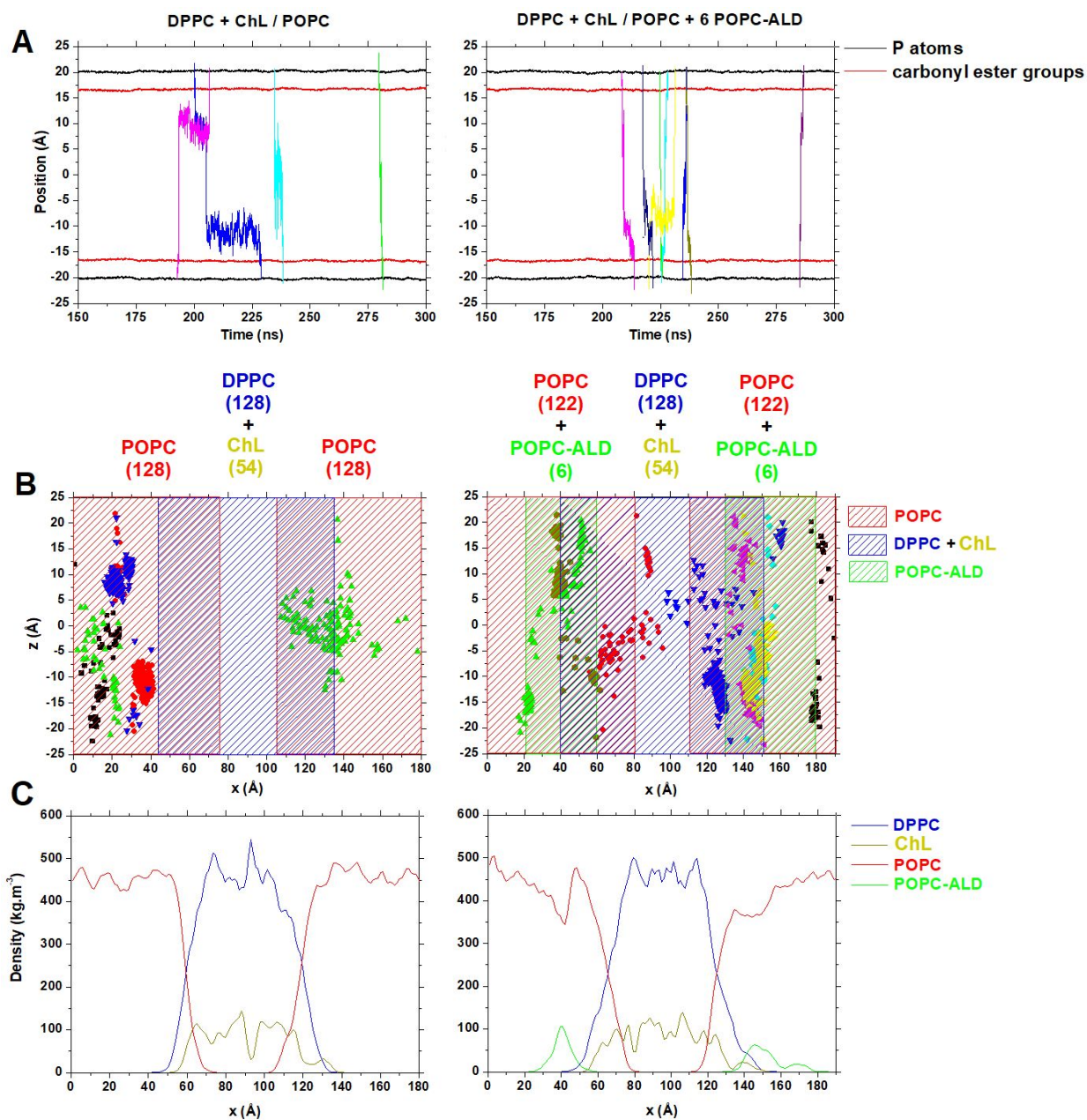
1
2
3
4 As mentioned in previous section, the increase in the membrane permeability can
5
6
7 be influenced by many factors, including the presence of oxidized lipids. Furthermore,
8
9
10 several studies have demonstrated that by exposing cells to pulsed electric fields
11
12
13 (electroporation), it is possible to increase their membrane permeability to ions and
14
15
16 various molecules, such as drugs and genes.^{66,67,68} Here, the membrane permeability
17
18
19 was evaluated by following the trajectory of all water molecules that cross the
20
21
22
23
24 membrane during the last 150 ns of simulation.
25
26
27

28
29 Remarkably, when only 6 POPC-ALD lipid molecules were added to each
30
31
32 domain interface (i.e., 5% of the lipids of each Ld domain, which corresponds to 1.5% of
33
34
35 the total lipids), the membrane permeability doubled. In other words, we counted 4
36
37
38 permeation events for the DPPC + ChL / POPC system and 8 permeation events for the
39
40
41
42 DPPC + ChL / POPC + 6 POPC-ALD system (Figure 7A). Moreover, in the latter
43
44
45
46 system, the water molecules spent less time at the membrane interior compared to the
47
48
49
50 DPPC + ChL / POPC system, meaning that the water molecules diffuse more easily
51
52
53
54 across the membrane in the DPPC + ChL / POPC + 6 POPC-ALD system. This
55
56
57
58
59
60

1
2
3
4 phenomenon is aligned with the fact that the shorter and highly mobile acyl chains of
5
6
7 lipid aldehydes are able to act as a water transporter. Interestingly, in the DPPC + ChL /
8
9
10 POPC system, most of the permeation events occurred at the bulk of the Ld domain
11
12
13 (Figure 7B). This can be correlated with the fluidity of the Ld domain. On the other hand,
14
15
16 in the DPPC + ChL / POPC + 6 POPC-ALD system, most of the permeation events
17
18
19 occurred both at the domain interfaces (POPC-ALD regions) and at the bulk of the Ld
20
21
22 domain (Figures 7B and 7C).
23
24
25
26
27
28

29 The addition of 6 POPC-ALD lipid molecules to each of the domain interfaces of
30
31
32 the DPPC + ChL / POPCOOH system increase the membrane permeability by a factor
33
34
35 of three: we counted 5 permeation events for the DPPC + ChL / POPCOOH system and
36
37
38 16 ± 3 permeation events for the DPPC + ChL / POPCOOH + 6 POPC-ALD system
39
40
41 (see Figure 8A and Figure S3B for DPPC + ChL / POPCOOH + 6 POPC-ALD system
42
43
44 replicates). In the absence of POPC-ALD, the permeation events occurred at the bulk of
45
46
47 the oxidized domain (Ld domain), while in the presence of POPC-ALD, most of them
48
49
50
51
52
53
54
55
56
57
58
59
60

occurred at the domain interfaces, as well at the bulk of the Ld domain (Figures 8B and 8C).



1
2
3
4 **Figure 7. (A)** Number of water permeation events calculated from the last 150 ns of
5
6
7 simulation to measure the effect caused by addition of POPC-ALD lipid molecules at
8
9
10 POPC domains. Each line color represents only one permeation event. **(B)** Two-
11
12 dimensional distribution of water permeation events over the last 150 ns of simulation.
13
14 Each symbol with specific color represents only one permeation event. **(C)** Density
15
16 profile along the *x*-axis calculated from the last 150 ns of simulation.
17
18
19
20
21
22
23
24
25
26
27
28
29
30
31
32
33
34
35
36
37
38
39
40
41
42
43
44
45
46
47
48
49
50
51
52
53
54
55
56
57
58
59
60

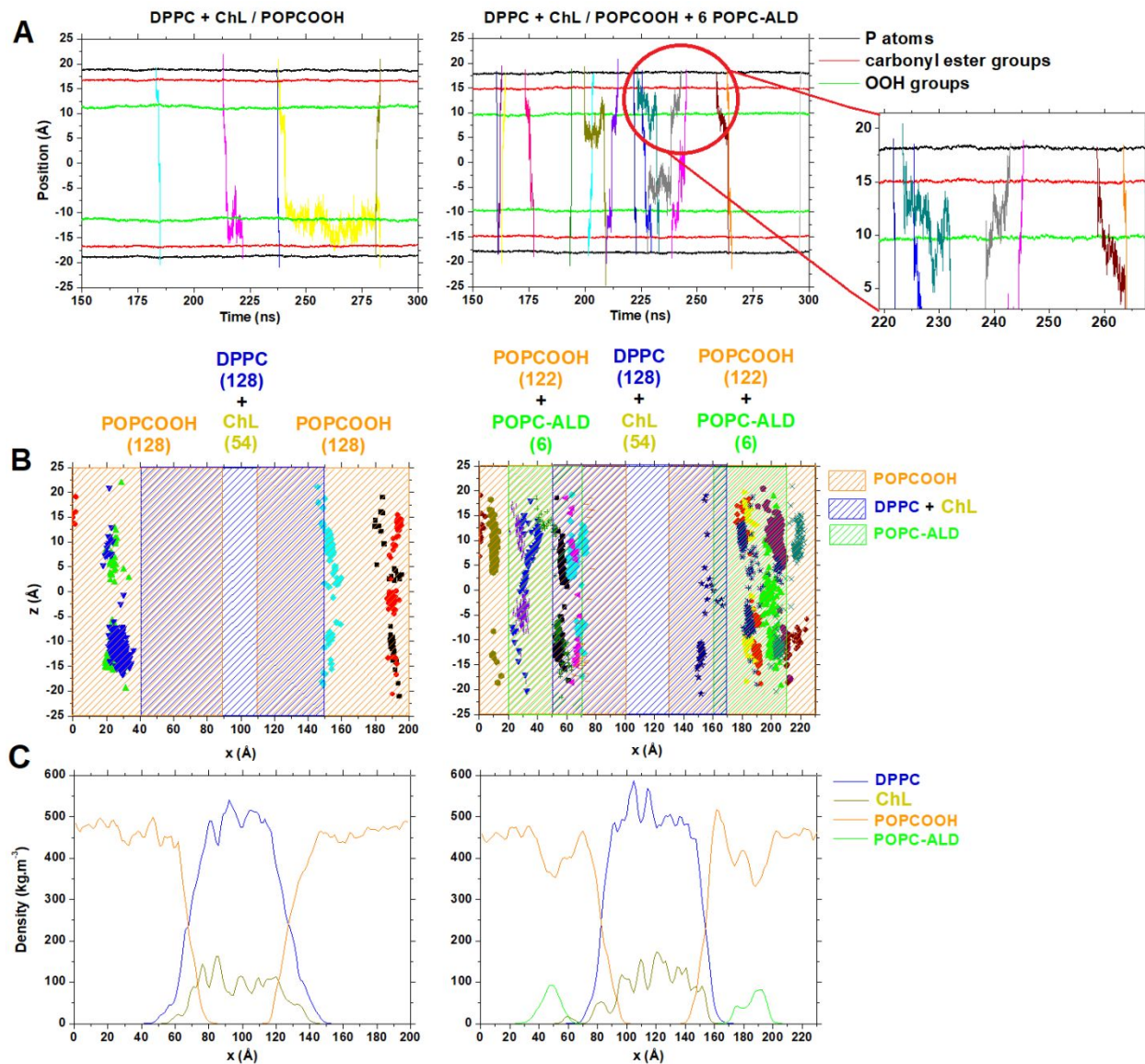


Figure 8. (A) Number of water permeation events calculated from the last 150 ns of simulation to measure the effect caused by addition of POPC-ALD lipid molecules at POPCOOH domains. Each line color represents only one permeation event. Some regions of the graphic on the right side were expanded, in order to show the propensity

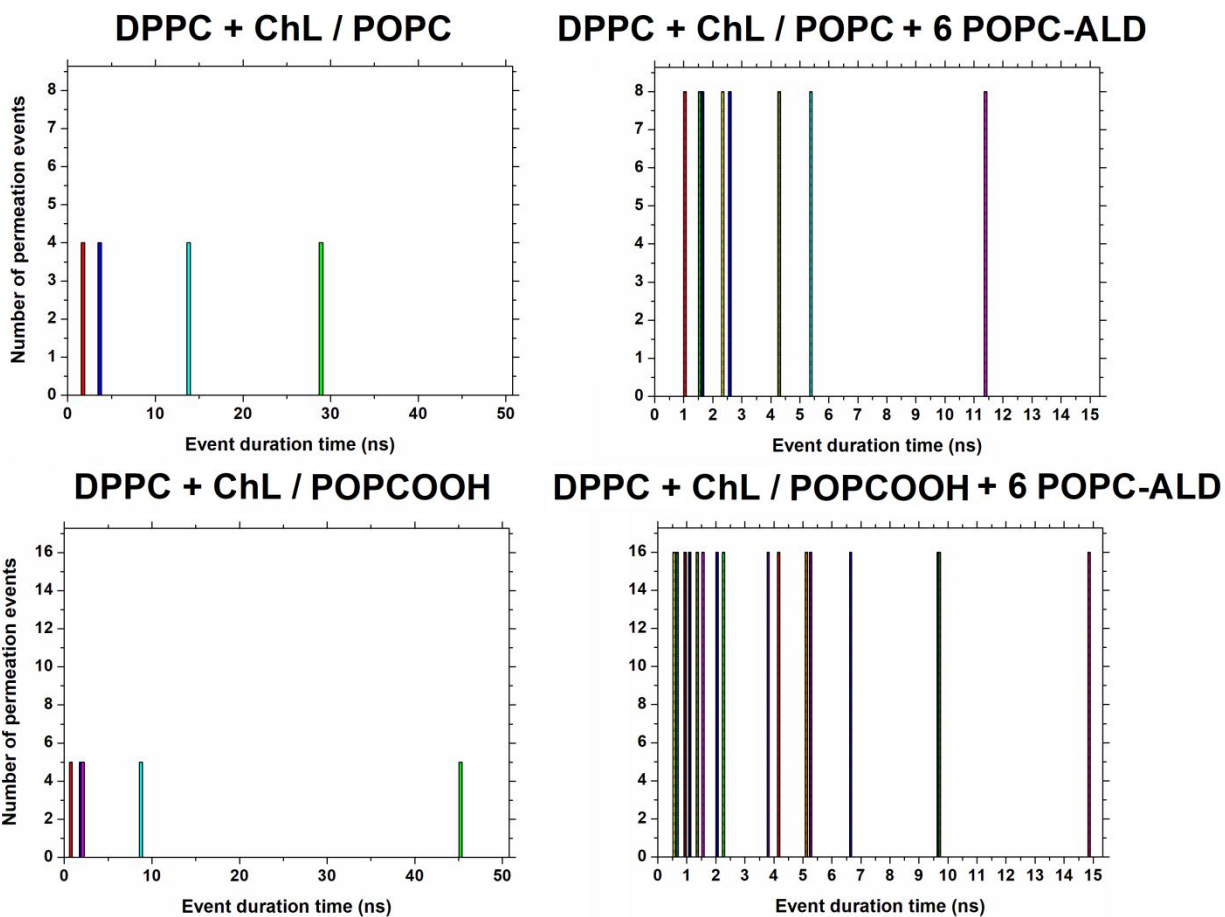
1
2
3 of the water molecules to spend time at the –OOH groups region. **(B)** Two-dimensional
4
5
6
7 distribution of water permeation events over the last 150 ns of simulation. Each symbol
8
9
10 with specific color represents only one permeation event. **(C)** Density profile at x -axis
11
12
13
14 calculated from the last 150 ns of simulation.
15
16
17
18
19
20
21
22

23 Permeation events are all very similar in both systems. Water molecules traverse
24
25
26 the headgroup region very rapidly, but get stuck for a few ns right below the headgroups
27
28
29 region, where they form H-bonds with the carbonyl ester groups. This tendency has
30
31
32 already been shown quantitatively in earlier simulation studies.⁴⁴ In the case of
33
34
35
36
37 POPCOOH lipids, the –OOH groups tend to migrate to the headgroup region⁶² and then
38
39
40 can interact with the water molecules. When water molecules detach from this region,
41
42
43 they diffuse across the membrane interior relatively fast. We can see in Figure 9 the
44
45
46 duration time (Δt) of the permeation events. Note that in the absence of POPC-ALD
47
48
49 lipids we have only a few permeation events. On the other hand, in the presence of
50
51
52
53
54 POPC-ALD lipids we have much more permeation events with shorter retention time at
55
56
57
58
59
60

1
2
3 the carbonyl ester and –OOH groups. Thus, the results suggest a mechanistic picture,
4
5
6 according to which the truncated chain of POPC-ALD lipids facilitates water permeation
7
8
9
10 across the interior membrane.
11
12
13

14
15 These results suggest that a few lipid aldehydes at the domain interface regions
16
17
18 (1.5% of the total lipids) are able to increase the membrane permeability. Wiczew and
19
20
21 co-workers showed that a small area of a cell membrane (with or without cholesterol)
22
23
24 oxidized with lipid aldehydes, would induce the formation of wide enough pores (up to ~
25
26
27
28 5 nm diameter) to transport ions and large molecules.⁶⁹ Moreover, they showed that the
29
30
31 membrane fluidity and the location of the “oxidative spots” might significantly affect the
32
33
34 pore’s lifespan.⁶⁹ However, the question arises: is the POPC-ALD-induced
35
36
37 permeabilization stronger at the interface between domains or in the bulk of Ld region?
38
39
40
41
42 To answer this question, we simulated single-phase membranes with the same number
43
44
45 of POPC-ALD molecules randomly distributed. Our aim was to determine whether the
46
47
48 presence of a few lipid aldehyde molecules is enough to increase the membrane
49
50
51
52
53
54
55
56
57
58
59
60

1
2
3 permeability in homogeneous POPC or POPCOOH membranes without pre-formed
4
5
6
7 domains.
8
9



10
11
12
13
14
15
16
17
18
19
20
21
22
23
24
25
26
27
28
29
30
31
32
33
34
35
36
37
38
39
40
41
42
43 **Figure 9.** Quantification of the permeation time for the model membranes. Each color
44 bar indicates a duration time of a permeation event. These events were calculated from
45
46
47
48
49
50
51
52
53
54
55
56
57
58
59
60
the last 150 ns of simulation.

1
2
3
4 Our results revealed that the addition of 5% of POPC-ALD lipid molecules to a
5
6
7 non-oxidized homogeneous membrane composed of POPC lipid molecules, which
8
9
10 represents part of a Ld domain, was not enough to increase the membrane
11
12
13 permeability: the permeability remained the same as in the native POPC system (i.e., 3
14
15
16 permeation events in each system, see Figure S4A). On the other hand, as discussed
17
18
19 above, the addition of the same number of POPC-ALD lipid molecules at the POPC
20
21
22 domains of heterogeneous (DPPC + ChL / POPC) membrane was able to increase the
23
24
25 membrane permeability by a factor of two (Figures 7A). The same is true for the
26
27
28 addition of POPC-ALD lipid molecules to an oxidized homogeneous membrane
29
30
31 composed of POPCOOH lipid molecules. We found 7 permeation events for the
32
33
34 POPCOOH system and 3 ± 3 for the POPCOOH + 6 POPC-ALD system (Figure S5A).
35
36
37
38
39
40
41 As mentioned above, to check the reproducibility of the permeation data, the
42
43
44 POPCOOH + 6 POPC-ALD system was simulated in triplicate (see Table S1 and Figure
45
46
47
48 S3A). Thus, our results reveal that the presence of a few lipid aldehydes in
49
50
51 homogeneous membranes is not enough to increase the membrane permeability, but
52
53
54 their presence at the domain interfaces is able to do that.
55
56
57
58
59
60

1
2
3
4 It should be mentioned that the systems DPPC + ChL / POPCOOH + 6 POPC-
5
6
7 ALD and POPCOOH + 6 POPC-ALD were simulated in triplicates, because they
8
9
10 represent heterogeneous and homogeneous membranes, respectively. As is clear from
11
12
13
14 Figure S3, the number of permeation events are similar for each replica, particularly in
15
16
17 DPPC + ChL / POPCOOH + 6 POPC-ALD system, which is the main object of this
18
19
20 study. In this sense, the permeation results of other single systems should be
21
22
23
24 acceptable.
25
26
27
28

29 In summary, our results show that the presence of a few lipid aldehydes at
30
31
32 the domain interfaces increases the membrane permeability 2- to 3-fold. This result
33
34
35
36 can be reproduced even at longer simulation time (500 ns, see Figure S6) which
37
38
39 does not affect the average permeability. Thus, the chosen simulation time (300 ns)
40
41
42
43 in our study is sufficient to observe the water permeation events. The same is true
44
45
46
47 when elongating the interface region by increasing the number of lipids and water
48
49
50 molecules in the y -axis (Figure S7), revealing that the box size simulated herein is
51
52
53
54 large enough and does not influence the above mentioned permeation results. The
55
56
57
58
59
60

1
2
3 same does not occur when the lipid aldehydes are added randomly in
4
5
6
7 homogeneous membranes. The experimental methods that enable the detection of
8
9
10 lipid oxidation products in membranes, are able to detect only the average content
11
12
13 of oxidized species and hence cannot distinguish between uniform and localized
14
15
16
17 distribution of oxidized lipids.^{70,71,72}
18
19
20
21

22 Note that in our simulations we assumed that the lipid aldehydes accumulated at
23
24
25 the domain interfaces, rather than at the Ld domain. To confirm our assumption, we
26
27
28 performed coarse-grained (CG) MD simulations, with initial random distribution of lipid
29
30
31 aldehydes, to evaluate their lateral diffusion, phase separation and the spontaneous
32
33
34 partitioning of them between different phases, over a long simulation time (see Figures
35
36
37 S8 and S9). We studied model membranes with two different lipid aldehydes, i.e., either
38
39
40 derived from POPC lipids (POPC-ALD) or derived from DIPC (1,2-dilinoleoyl-sn-glycero-
41
42
43 3-phosphocholine) lipids (DIPC-ALD). Indeed, our CG simulations demonstrated that
44
45
46
47 the POPC-ALD lipids tend to accumulate at the interface between domains (Figures S8
48
49
50
51
52
53
54
55
56
57
58
59
60

1
2
3 and S10), but the same does not occur for DIPC-ALD lipids, which remain at the Ld
4
5
6
7 phase (Figures S9 and S10).
8
9

10
11 To understand the above mentioned effects, future investigations are required,
12
13 which help to determine if the interfacial activity is driven by either lipid geometry or
14
15 interactions between saturated and unsaturated lipid acyl chains of the lipid aldehydes
16
17
18 with the Lo and Ld domains. It is noteworthy that coarse-grained models have been
19
20
21 successfully used for showing interfacial accumulation of certain lipid types,⁷³ and that
22
23
24 such an effect would help to explain why minute lipid aldehyde amounts are able to
25
26
27 cause an order-of-magnitude alteration in membrane permeability.⁵⁸
28
29
30
31
32
33
34
35

36 CONCLUSIONS

37
38
39
40

41 We presented an atomistic view of how lipid oxidation affects the permeability of
42
43
44 phase-separated domains in model membranes, where the Lo domain was composed
45
46
47 of DPPC + ChL molecules and the Ld domain was composed of either POPC or
48
49
50 POPCOOH lipid molecules. We also evaluated the effect of the addition of lipid
51
52
53 aldehydes at the Lo/Ld domain interfaces. Only 5% of lipid aldehydes alone were not
54
55
56
57
58
59
60

1
2
3 enough to increase the membrane permeability when distributed randomly in single-
4
5
6
7 phase membranes. However, their presence at the Lo/Ld domain interfaces (1.5% of
8
9
10 the total lipids) was able to increase the permeability by 2- and 3-fold for non-oxidized
11
12
13 and oxidized lipids at the Ld domain, respectively. This might help to explain why minute
14
15
16
17 lipid aldehyde amounts at domain interfaces are able to drastically increase the
18
19
20
21 membrane permeability. This study is of interest for photodynamic therapy and plasma
22
23
24
25 medicine for cancer treatment, to understand the effects caused by free radicals in cell
26
27
28 membranes.
29
30
31
32
33
34
35
36
37
38
39
40
41
42
43
44
45
46
47
48
49

50 ASSOCIATED CONTENT

51
52
53

54 Supporting Information

55
56
57
58
59
60

1
2
3
4 Molecular topology files (.itp) for the atomistic models (DPPC, ChL, POPC, POPCOOH,
5
6
7 POPC-ALD) and CG models (DPPC, ChL, DIPC, POPC-ALD, DIPC-ALD); Molecular
8
9
10 coordinates (.gro) for all systems at 300 ns; Inputs (.inp) for Packmol (ZIP); Membrane
11
12
13 structural properties (Tables S1 and S2); Membrane equilibration (Figure S1);
14
15
16
17 Membrane interface (Figure S2); Membrane permeation events (Figures S3-S7); CG
18
19
20
21 results (Figures S8-S10) (PDF).
22
23
24

25 **Data and Software Availability**

26
27
28

29 GROMACS is free software to perform MD simulations. The GROMACS package
30
31
32
33 version 5.1.2 can be downloaded at
34
35
36 <https://manual.gromacs.org/documentation/5.1.2/download.html>.
37
38
39

40
41 Packmol is also free software which creates initial structures for MD simulations by
42
43
44 packing molecules in defined regions of space (defined by the user). The user must
45
46
47
48 provide only the coordinates of one molecule of each type, the number of molecules of
49
50
51 each type and the spatial constraints that each type of molecule must satisfy. We
52
53
54
55 provide in the Supporting Information the inputs used to build up our lipid bilayers (ZIP).
56
57
58
59
60

1
2
3 The Packmol can be downloaded at

4
5
6
7 <http://m3g.igmm.unicamp.br/packmol/download.shtml>.

8
9
10
11 VMD is also free software for displaying, animating, and analyzing large biomolecular
12 systems using 3D graphics. The VMD package version 1.9.3 can be downloaded at

13
14
15
16
17 <https://www.ks.uiuc.edu/Development/Download/download.cgi?PackageName=VMD>.

18
19
20
21
22 SuAVE is also free software to calculate the surface curvature of chemical systems, as
23 well several curvature-dependent properties like area per lipid, density, order
24 parameter, volume per lipid, and so on. These quantities can be represented either as
25 time-dependent or space- and time-averaged projections over topographical (2D) maps.

26
27
28
29
30
31
32
33
34
35
36 The SuAVE can be downloaded at <https://www.biomatsite.net/suave-software>.

37
38
39
40
41
42
43
44
45
46
47
48
49
50
51
52
53
54
55
56
57
58
59
60
The program used to calculate our membrane permeability detects spontaneous permeation events of water molecules through the lipid bilayer, characterizing its crossing time and trajectory at coordinates x , y and z . This software can be obtained contacting the authors.⁵⁷

1
2
3
4
5
6
7 **AUTHOR INFORMATION**
8
9

10
11 **Corresponding Author**
12

13
14
15 *Email: rodrigo.cordeiro@ufabc.edu.br (Rodrigo M. Cordeiro)
16
17

18
19 **Author Contributions**
20

21
22
23 The manuscript was written through contributions of all authors. All authors have given
24
25
26 approval to the final version of the manuscript.
27
28

29
30
31 **Notes**
32

33
34
35 The authors declare no competing financial interest.
36
37
38

39 **ACKNOWLEDGMENT**
40

41
42 We thank Universidade Federal do ABC for providing the computational resources
43
44
45
46 needed for completion of this work and CAPES for the scholarship granted. M.Y.
47
48
49 acknowledges the Flanders Research Foundation (grant 1200219N) for financial
50
51
52
53 support.
54
55
56
57
58
59
60

REFERENCES

(1) van Meer, G.; Voelker, D. R.; Feigenson, G. W., Membrane lipids: where they are and how they behave, *Nat. Rev. Mol. Cell Biol.* 2008, 9, 112-124.

(2) Maccarrone, M.; Catani, M. V.; Agrò, A. F.; Melino, G., Involvement of 5-lipoxygenase in programmed cell death of cancer cells, *Cell Death Diff.* 1997, 4, 396-402.

(3) Frankel, E. N., Chemistry of Free Radical and Singlet Oxidation of Lipids, *Prog. Lipid Res.* 1985, 23, 197-221.

(4) Brodnitz, M. H.; Nawar, W. W.; Fagerson, I. S., Autoxidation of Saturated Fatty Acids. I. Initial Products of Autoxidation of Methyl Palmitate, *Lipids* 1968, 3, 59-64.

(5) Jurkiewicz, P.; Olzyska, A.; Cwiklik, L.; Conte, E.; Jungwirth, P.; Megli, F. M.; Hof, M., Biophysics of Lipid Bilayers Containing Oxidatively Modified Phospholipids: Insights

1
2
3 from Fluorescence and EPR Experiments and from MD Simulations, *Biochim. Biophys.*
4
5
6
7 *Acta* 2012, 1818, 2388-2402.

8
9
10
11 (6) Valko, M.; Leibfritz, D.; Moncol, J.; Cronin, M. T. D.; Mazur, M.; Telser, J., Free
12
13
14 radicals and Antioxidants in Normal Physiological Functions and Human Disease, *Int. J.*
15
16
17
18 *Biochem. Cell Biol.* 2007, 39, 44-84.

19
20
21
22 (7) Bradley-Whitman, M. A.; Lovell, M. A., Biomarkers of Lipid Peroxidation in Alzheimer
23
24
25
26 Disease (AD): an update, *Arch. Toxicol.* 2015, 89, 1035-1044.

27
28
29
30 (8) Munir, R.; Lisek, J.; Swinnen, J. V.; Zaidi, N., Lipid Metabolism in Cancer Cells under
31
32
33
34 Metabolic Stress, *Br. J. Cancer* 2019, 120, 1090-1098.

35
36
37
38 (9) Singer, S. J.; Nicolson, G. L., The Fluid Mosaic Model of the Structure of Cell
39
40
41
42 Membranes, *Science* 1972, 175, 220-731.

43
44
45
46 (10) Simons, K.; Sampaio, J. L., Membrane Organization and Lipid Rafts, *Cold Spring*
47
48
49
50 *Harb. Perspect. Biol.* 2011, 3, a004697.

1
2
3
4 (11) Lingwood, D.; Simons, K., Lipid Rafts as a Membrane-Organizing Principle,
5
6
7 Science 2010, 327, 46-50.
8
9

10
11 (12) Van der Paal, J.; Hong, S-H.; Yusupov, M.; Gaur, N.; Oh, J-S.; Short, R. D.; Szili,
12
13
14 E. J.; Bogaerts, A., How membrane lipids influence plasma delivery of reactive oxygen
15
16
17
18 species into cells and subsequent dna damage: an experimental and computational
19
20
21
22 study, Phys. Chem. Chem. Phys. 2019, 21, 19327-19341.
23
24
25

26 (13) Simons, K.; Ikonen, E., Functional Rafts in Cell Membranes, Nature 1997, 387,
27
28
29
30 569-572.
31
32

33
34 (14) Simons K.; Toomre, D., Lipid Rafts and Signal Transduction, Nat. Rev. Mol. Cell
35
36
37
38 Bio. 2000, 1, 31-39.
39
40

41
42 (15) Veatch, S. L.; Sengupta, P.; Honerkamp-Smith, A. R.; Holowka, D.; Baird, B.,
43
44
45
46 Critical fluctuations in plasma membrane vesicles, ACS Chem. Biol. 2008, 3, 287-293.
47
48
49
50
51
52
53
54
55
56
57
58
59
60

1
2
3
4 (16) Rayermann, S. P.; Rayermann, G. E.; Cornell, C. E.; Merz, A. J.; Keller, S. L.,
5
6
7 Hallmarks of reversible separation of living, unperturbed cell membranes into two liquid
8
9
10 phases, *Biophys. J.* 2017, 113, 2425-2432.

11
12
13
14
15 (17) King, C.; Sengupta, P.; Seo, A.Y.; Lippincott-Schwarz, J., ER membranes exhibit
16
17
18 phase behavior at sites of organelle contact, *Proc. Natl. Acad. Sci. U.S.A.* 2020, 117,
19
20
21 7225-7234.

22
23
24
25
26 (18) Machta, B. B.; Papanikolaou, S.; Sethna, J. P.; Veatch, S. L., Minimal model of
27
28
29 plasma membrane heterogeneity requires coupling cortical actin to criticality, *Biophys.*
30
31
32
33
34
35
36
37
38
39
40
41
42
43
44
45
46
47
48
49
50
51
52
53
54
55
56
57
58
59
60
J. 2011, 100, 1668-1677.

59
60
(19) Miller, E. J.; Ratajczak, A. M.; Anthony, A. A.; Mottau, M.; Gonzalez, X. I. R.;
Honerkamp-Smith, A. R., Divide and conquer: How phase separation contributes to
lateral transport and organization of membrane proteins and lipids, *Chem. Phys. Lipids*
2020, 233, 104985.

1
2
3
4 (20) Arumugam, S.; Petrov, E. P.; Schwille, P., Cytoskeletal Pinning Controls Phase
5
6
7 Separation in Multicomponent Lipid Membranes, *Biophys. J.* 2015, 108 1104-1113.
8

9
10
11 (21) Aresta-Branco, F.; Cordeiro, A.M.; Marinho, H.S.; Cyrne, L.; Antunes, F.; de
12
13
14 Almeida, R. F. M., Gel Domains in the Plasma Membrane of *Saccharomyces*
15
16
17
18 *Cerevisiae*, *J. Biol. Chem.* 2011, 286, 5043-5054.
19

20
21
22 (22) Vecer, J.; Vesela, P.; Malinsky, J.; Herman P., Sphingolipid Levels Crucially
23
24
25
26 Modulate Lateral Microdomain Organization of Plasma Membrane in Living Yeast,
27
28
29
30 *FEBS Lett.* 2014, 588, 443-449.
31

32
33
34 (23) Haluska, C. K.; Baptista, M.S.; Fernandes, A. U.; Schroder, A. P.; Marques, C. M.;
35
36
37
38 Itri, R., Photo-activated Phase Separation in Giant Vesicles made from Different Lipid
39
40
41
42 Mixtures, *Biochim. Biophys. Acta-Biom.* 2012, 1818, 666-672.
43

44
45 (24) Israelachvili, J. N.; Mitchell, D. J., A Model for the Packing of Lipids in Bilayer
46
47
48
49
50
51
52
53
54
55
56
57
58
59
60 Membranes, *Biochim. Biophys. Acta* 1975, 389, 13-19.

1
2
3
4 (25) Tsubone, T. M.; Junqueira, H. C.; Baptista, M. S.; Itri, R., Contrasting Roles of
5
6
7 Oxidized Lipids in Modulating Membrane Microdomains, *Biochim. Biophys. Acta-Biom.*
8
9
10 2019, 1861, 660-669.

11
12
13
14
15 (26) Koynova, R.; Caffrey, M., Phases and Phase Transitions of the
16
17
18 Phosphatidylcholines, *Biochim. Biophys. Acta* 1998, 1376, 91-145.

19
20
21
22
23 (27) Jones, J. W.; Lue, L.; Saiani, A.; Tiddy, G. J. T., Density, DSC, X-ray and NMR
24
25
26 measurements through the gel and lamellar phase transitions of 1-myristoyl-2-stearoyl-
27
28
29 sn-glycero-3-phosphatidylcholine (MSPC) and 1-stearoyl-2-myristoyl-sn-glycero-3-
30
31
32 phosphatidylcholine (SMPC): observation of slow relaxation processes and
33
34
35 mechanisms of phase transitions, *Phys. Chem. Chem. Phys.* 2012, 14, 5452-5469.

36
37
38
39
40
41 (28) Cordeiro, R. M., Molecular Structure and Permeability at the Interface between
42
43
44 Phase-Separated Membrane Domains, *J. Phys. Chem. B* 2018, 122, 6954-6965.

45
46
47
48
49 (29) Papahadjopoulos, D.; Jacobson, K.; Isac, T., Phase Transitions in Phospholipid
50
51
52 Vesicles: Fluorescence Polarization and Permeability Measurements Concerning the
53
54
55

1
2
3 Effect of Temperature and Cholesterol, *Biochim. Biophys. Acta-Biom.* 1973, 311, 330-
4
5
6
7 348.

8
9
10
11 (30) Heimburg, T., *Lipid Ion Channels*, *Biophys. Chem.* 2010, 150, 2-22.

12
13
14
15
16 (31) Wu, H. L.; Sheng, Y. J.; Tsao, H. K., *Phase Behaviors and Membrane Properties of*
17
18
19 *Model Liposomes: Temperature Effect*, *J. Chem. Phys.* 2014, 141, 124906.

20
21
22
23
24 (32) Ghysels, A.; Krämer, A.; Venable, R. M.; Jr, W. E. T.; Lyman, E.; Gawrisch, K.;
25
26
27 Pastor, R. W., *Permeability of membranes in the liquid ordered and liquid disordered*
28
29
30 *phases*, *Nat. Comm.* 2019, 10, 5616.

31
32
33
34
35 (33) Yusupov, M.; Wende, K.; Kupsch, S.; Neyts, E. C.; Reuter, S.; Bogaerts, A., *Effect*
36
37
38 *of head group and lipid tail oxidation in the cell membrane revealed through integrated*
39
40
41 *simulations and experiments*, *Sci. Reports* 2017, 7, 5761.

42
43
44
45
46 (34) Ayee, M. A. A.; LeMaster E.; Shentu, T. P.; Singh, D. K.; Barbera, N.; Soni, D.;
47
48
49
50 *Tiruppathi, C.; Subbaiah, P. V.; Berdyshev, E.; Bronova, I.; Cho, M.; Akpa, B. S.;*

1
2
3
4 Levitan, I., Molecular-scale Biophysical Modulation of an Endothelial Membrane by
5
6
7 Oxidized Phospholipid, *Biophys. J.* 2017, 112, 325-338.
8
9

10
11 (35) Oliveira, M. C.; Yusupov, M.; Bogaerts, A.; Cordeiro, R. M., How do Nitrated Lipids
12
13
14 affect the Properties of Phospholipid Membranes?, *Arch. Biochem. Biophys.* 2020, 695,
15
16
17
18 108548.
19

20
21
22
23 (36) Boonnoy, P.; Jarerattanachat, V.; Karttunen, M.; Wong-ekkabut, J., Bilayer
24
25
26 Deformation, Pores, and Micellation Induced by Oxidized Lipids, *J. Phys. Chem. Lett.*
27
28
29
30 2015, 6, 4884-4888.
31

32
33
34 (37) Van der Paal, J.; Neyts, E. C.; Verlackt, C. C. W.; Bogarts, A., Effect of Lipid
35
36
37 Peroxidation on Membrane Permeability of Cancer and Normal Cells Subjected to
38
39
40
41 Oxidative Stress, *Chem. Sci.* 2016, 7, 489-498.
42
43

44
45
46 (38) Bacellar, I. O. L.; Tsubone, T. M.; Pavani, C.; Baptista, M. S., Photodynamic
47
48
49 Efficiency: From Molecular Photochemistry to Cell Death, *Int. J. Mol. Sci.* 2015, 16,
50
51
52
53 20523-20559.
54

1
2
3
4 (39) Robert, E.; Darny, T.; Dozias, S.; Iseni, S.; Pouvesle, J. M., New insights on the
5
6
7 propagation of pulsed atmospheric plasma streams: from single jet to multi jet arrays,
8
9
10 Phys. Plasmas 2015, 22, 122007.

11
12
13
14
15 (40) Hirst, A. M.; Frame, F. M.; Arya, M.; Maitland, N. J.; O'Connell, D., Low
16
17
18 temperature plasmas as emerging cancer therapeutics: the state of play and thoughts
19
20
21 for the future, Tumour Biol. 2016, 37, 1-11.

22
23
24
25
26 (41) van der Spoel, D.; Lindah, E.; Hess, B.; Groenho, G.; Mark, A. E.; Berendsen, H. J.
27
28
29 C., GROMACS: Fast, Flexible, and Free, J. Comput. Chem. 2005, 26, 1701-1718.

30
31
32
33
34 (42) Oostenbrink, C.; Villa, A.; Mark, A. E.; Van Gunsteren, W. F., A Biomolecular Force
35
36
37 Field Based on the Free Enthalpy of Hydration and Solvation: The GROMOS Force-field
38
39
40 Parameter sets 53A5 and 53A6, J. Comput. Chem. 2004, 25, 1656-1676.

41
42
43
44
45 (43) Poger, D.; Mark, A. E., On the Validation of Molecular Dynamics Simulations of
46
47
48 Saturated and cis-monounsaturated Phosphatidylcholine Lipid Bilayers: A Comparison
49
50
51 with Experiment. J. Chem. Theory Comput. 2010, 6, 325-336.
52
53
54
55
56
57
58
59
60

1
2
3
4 (44) Neto, A. J. P.; Cordeiro, R. M., Molecular Simulations of the Effects of Phospholipid
5
6
7 and Cholesterol Peroxidation on Lipid Membrane Properties, *Biochim. Biophys. Acta-*
8
9
10 *Biom.* 2016, 1858, 2191-2198.

11
12
13
14
15 (45) Petrov, D.; Margreitter, C.; Grandits, M.; Oostenbrink, C.; Zagrovic, B., A
16
17
18 systematic framework for molecular dynamics simulations of protein post-translational
19
20
21 modifications, *PLoS Comput. Bio.* 2013, 9, e1003154.

22
23
24
25
26 (46) Oostenbrink, C.; Soares, T. A.; van der Vegt, N. F. A.; van Gunsteren, W. F.,
27
28
29 Validation of the 53A6 GROMOS force field, *Eur. Biophys. J.* 2005, 34, 273-284.

30
31
32
33
34 (47) Martinez, L.; Andrade, R.; Birgin, E. G.; Martinez, J. M., Packmol: A package for
35
36
37 Building Initial Configurations for Molecular Dynamics Simulations, *J. Comput. Chem.*
38
39
40 2009, 30, 2157-2164.

41
42
43
44
45 (48) Humphrey, W.; Dalke, A.; Schulten, K., VMD: Visual Molecular Dynamics, *J. Mol.*
46
47
48 *Graphics* 1996, 14, 33-38.

1
2
3
4 (49) Gardner, H. W., Oxygen Radical Chemistry of Polyunsaturated Fatty Acids, Free
5
6
7 Radical Biol. Med. 1989, 7, 65-86.

8
9
10
11 (50) Berendsen, H. J. C.; Postma, J. P. M.; van Gunsteren, W. F.; Hermans, J.,
12
13
14 Interaction Models for Water in Relation to Protein Hydration, in: Intermolecular Forces,
15
16
17 Dordrecht: B. Pullman 1981, 331-342.

18
19
20
21
22
23 (51) Nose, S., A molecular-dynamics method for simulations in the canonical ensemble,
24
25
26 Mol. Phys. 1984, 52, 255-268.

27
28
29
30
31 (52) Hoover, W. G., Canonical dynamics - equilibrium phase-space distributions, Phys.
32
33
34 Rev. A 1985, 31, 1695-1697.

35
36
37
38
39 (53) Parrinello, M.; Rahman, A., Polymorphic Transitions in Single-Crystals - A new
40
41
42 molecular-dynamics method, J. Appl. Phys. 1981, 52, 7182-7190.

43
44
45
46
47 (54) Raudino, A.; Zuccarello, F.; La Rosa, C.; Buemi, G., Thermal expansion and
48
49
50 compressibility coefficients of phospholipid vesicles: experimental determination and
51
52
53 theoretical modeling, J. Phys. Chem. 1990, 94, 4217-4223.

1
2
3
4 (55) Rycroft, C. H., VORO++: A three-dimensional Voronoi cell library in C++, Chaos
5
6
7 2009, 19, 041111.
8
9

10
11 (56) Santos, D. E. S.; Pontes, F. J. S.; Lins, R. D.; Coutinho, K.; Soares, T. A., SuAVE:
12
13
14 A Tool for Analyzing Curvature-Dependent Properties in Chemical Interfaces, J. Chem.
15
16
17
18 Inf. Model. 2020, 60, 473-484.
19
20
21

22
23 (57) Camilo, C. R. S.; Ruggiero, J. R.; de Araujo, A. S., A Method for Detection of
24
25
26 Permeation Events in Molecular Dynamics Simulations of Lipid Bilayers. bioRxiv 2021,
27
28
29
30 DOI: 10.1101/2021.01.20.427278.
31
32

33
34 (58) Runas, K. A.; Malmstadt, N., Low levels of lipid oxidation radically increase the
35
36
37
38 passive permeability of lipid bilayers, Soft Matter 2015, 11, 499-505.
39
40

41
42 (59) Bennett, W. F. D.; Tieleman, D. P., Computer Simulations of Lipid Membrane
43
44
45
46 Domains, Biochim. Biophys. Acta 2013, 1828, 1765-1776.
47
48

49
50 (60) Carpenter, T. S.; López, C. A.; Neale, C.; Montour, C.; Ingólfsson, H. I.; Di Natale,
51
52
53
54 F.; Lightstone, F. C.; Gnanakaran, S., Capturing Phase Behavior of Ternary Lipid
55
56
57

1
2
3
4 Mixtures with a Refined Martini Coarse-Grained Force Field, *J. Chem. Theory Comput.*
5
6
7 2018, 14, 6050-6062.
8
9

10
11 (61) Kučerka, N.; Nieh, M.; Katsaras, J., Fluid Phase Lipid Areas and Bilayer
12
13
14
15 Thicknesses of Commonly used Phosphatidylcholines as a Function of Temperature,
16
17
18 *Biochim. Biophys. Acta* 2011, 1808, 2761-2771.
19
20

21
22
23 (62) Weber, G.; Charitat, T.; Baptista, M. S.; Uchoa, A. F.; Pavani, C.; Junqueira, H. C.;
24
25
26 Guo, Y.; Baulin, V. A.; Itri, R.; Marques, C. M.; Schroder, A. P., Lipid Oxidation Induces
27
28
29
30 Structural Changes in Biomimetic Membranes, *Soft Matter* 2014, 10, 4241-4247.
31
32

33
34 (63) Beranova, L.; Cwiklik, L.; Jurkiewicz, P.; Hof, M.; Jungwirth, P., Oxidation Changes
35
36
37
38 Physical Properties of Phospholipid Bilayers: Fluorescence Spectroscopy and Molecular
39
40
41 Simulations, *Langmuir* 2010, 26, 6140-6144.
42
43

44
45
46 (64) De Rosa, R.; Spinozzi, F.; Itri, R., Hydroperoxide and Carboxyl Groups Preferential
47
48
49
50 Location in Oxidized Biomembranes Experimentally Determined by Small Angle X-Ray
51
52

1
2
3
4 Scattering: Implications in Membrane, *Biochim. Biophys. Acta-Biom.* 2018, 1860, 2299-
5
6
7 2307.

8
9
10
11 (65) Yesylevskyy, S.; Rivel, T.; Ramseyer, C., Curvature increases permeability of the
12
13
14 plasma membrane for ions, water and the anti-cancer drugs cisplatin and gemcitabine,
15
16
17
18 *Scientific Reports* 2019, 9, 17214.

19
20
21
22 (66) Hanna, H.; Denzi, A.; Liberti, M.; André, F. M.; Mir, L. M., Electroporation of
23
24
25
26 Inner and Outer Cell Membranes with Microsecond Pulsed Electric Fields: Quantitative
27
28
29
30 Study with Calcium Ions, *Scientific Reports* 2017, 7, 1-14.

31
32
33 (67) Pasquet, L.; Chabot, S.; Bellard, E.; Rols, M. P.; Teissie, J.; Golzio, M.,
34
35
36
37
38 Noninvasive Gene Electrotransfer in Skin, *Human Gene Therapy Methods* 2019, 30, 17-
39
40
41 22.

42
43
44 (68) Bo, W.; Silkunas, M.; Mangalanathan, U.; Novickij, V.; Casciola, M.; Semenov, I.;
45
46
47
48
49 Xiao, S.; Pakhomova, O. N.; Pakhomov, A. G., Probing Nanoelectroporation and
50
51

1
2
3 Resealing of the Cell Membrane by the Entry of Ca²⁺ and Ba²⁺ Ions, *Int. J. Mol. Sci.*
4
5
6
7 2020, 21, 3386.

8
9
10
11 (69) Wiczew, D.; Szulc, N.; Tarek, M., On the Permeability of Cell Membranes
12
13
14
15 Subjected to Lipid Oxidation, DOI: <https://doi.org/10.1101/2020.11.30.403345>.

16
17
18
19 (70) Drummen, G. P. C.; Gadella, B. M.; Post, J. A.; Brouwers, J. F., Mass
20
21
22
23 Spectrometric Characterization of the Oxidation of the Fluorescent Lipid Peroxidation
24
25
26 Reporter Molecule C11-BODIPY581/591, *Free Radical Biol. Med.* 2004, 36, 1635-1644.

27
28
29
30
31 (71) Kaur, A.; Kolanowski, J. L.; New, E. J., Reversible Fluorescent Probes for
32
33
34
35 Biological Redox States, *Angew. Chem. Int. Ed.* 2016, 55, 1602–1613.

36
37
38
39 (72) Michel, O.; Pakhomov, A. G.; Casciola, M.; Saczko, J.; Kulbacka, J.; Pakhomova,
40
41
42 O. N., Electroporabilization does not Correlate with Plasma Membrane Lipid
43
44
45
46 Oxidation, *Bioelectrochem.* 2020, 132, 107433.

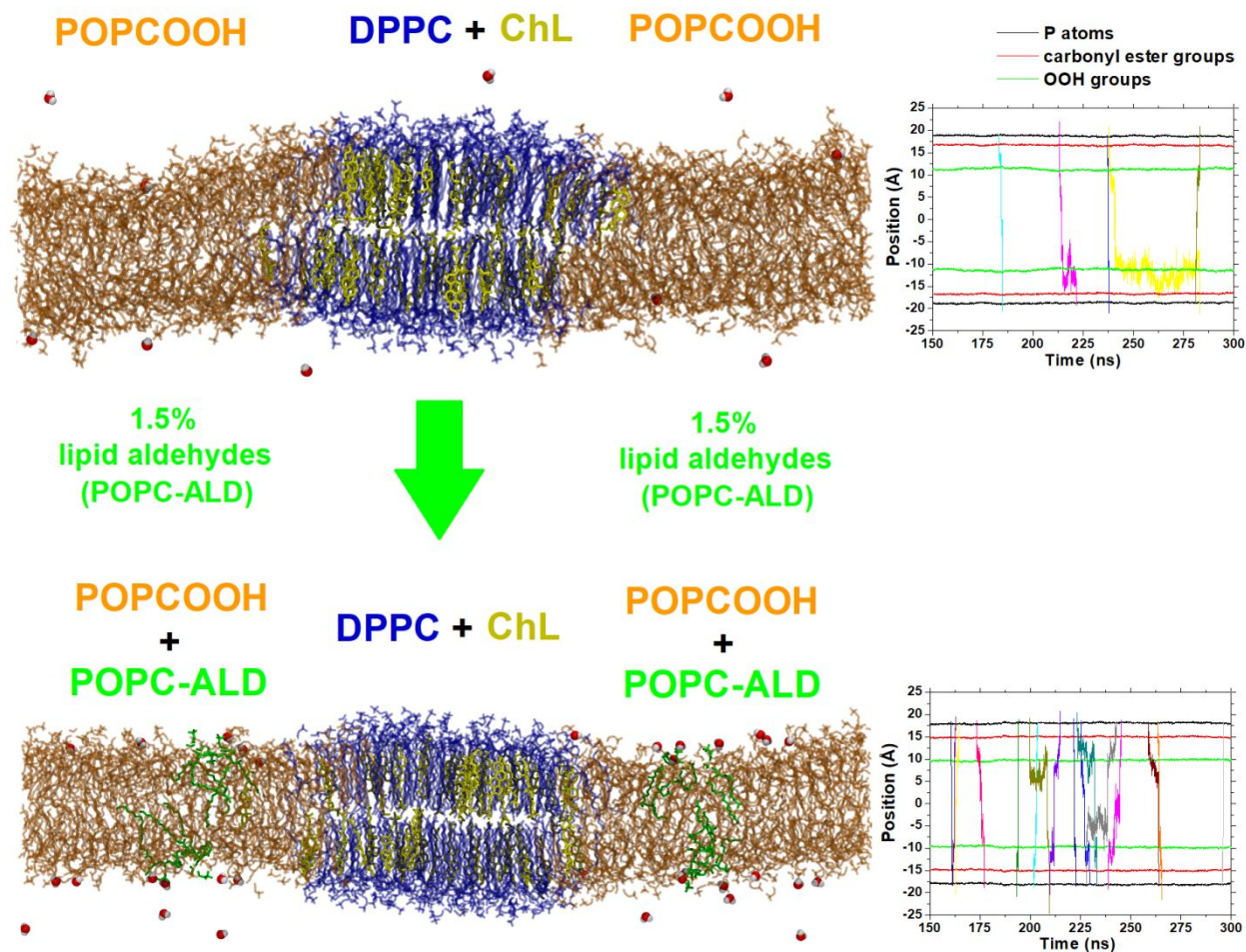
47
48
49
50 (73) Schafer, L. V.; Marrink, S. J., Partitioning of Lipids at Domain Boundaries in Model
51
52
53
54 Membranes, *Biophys. J.* 2010, 99, L91-L93.

1
2
3
4
5
6
7
8
9
10
11
12
13
14
15
16
17
18
19
20
21
22
23
24
25
26
27
28
29
30
31
32
33
34
35
36
37
38
39
40
41
42
43
44
45
46
47
48
49
50
51
52
53
54
55
56
57
58
59
60

For Table of Contents Only

Lipid Oxidation: Role of Membrane Phase-Separated
Domains

*Maria C. Oliveira, Maksudbek Yusupov, Annemie Bogaerts, Rodrigo M. Cordeiro**



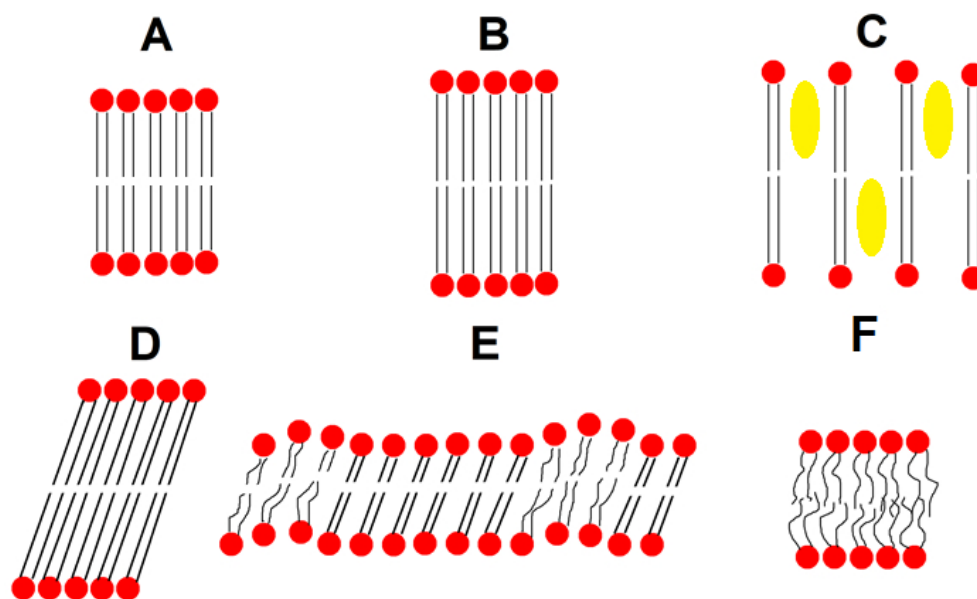


Figure 1. Schematic representation of the various lamellar lipid phases: (A) crystalline lamellar subgel (L_c); (B) gel with untilted chains (L_{α}); (C) liquid-ordered (L_o), where the filled oval circles in yellow represent cholesterol molecules; (D) gel with tilted chains (L_{α}'); (E) rippled gel (P_{α}') and (F) liquid crystalline (L_{α}).

186x113mm (96 x 96 DPI)

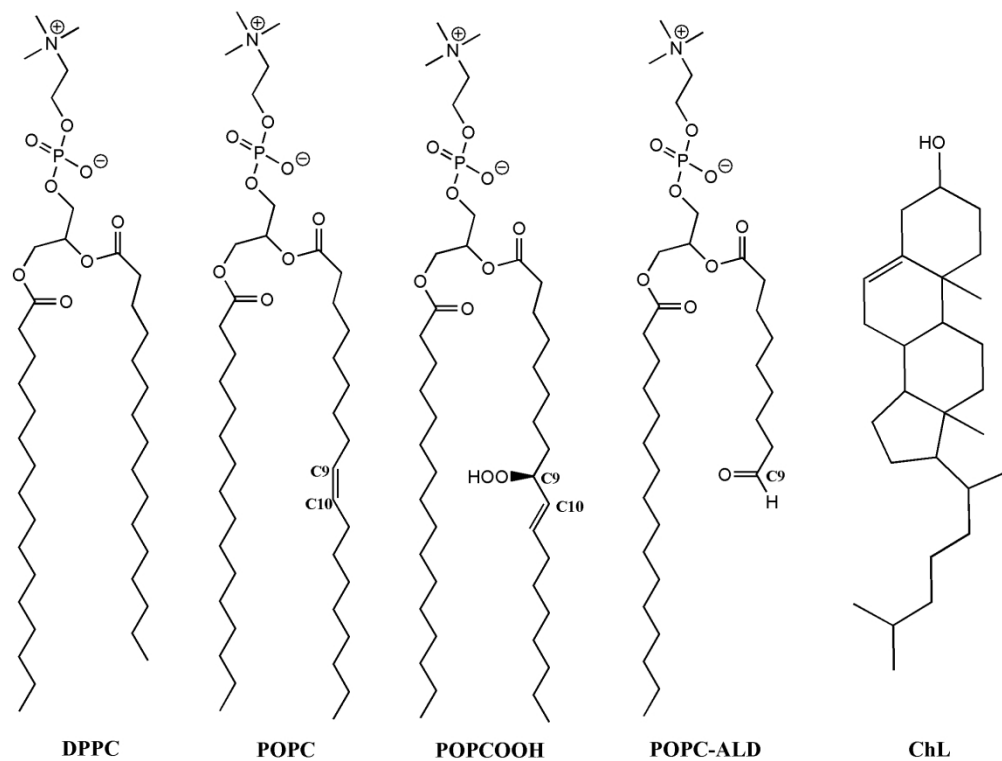
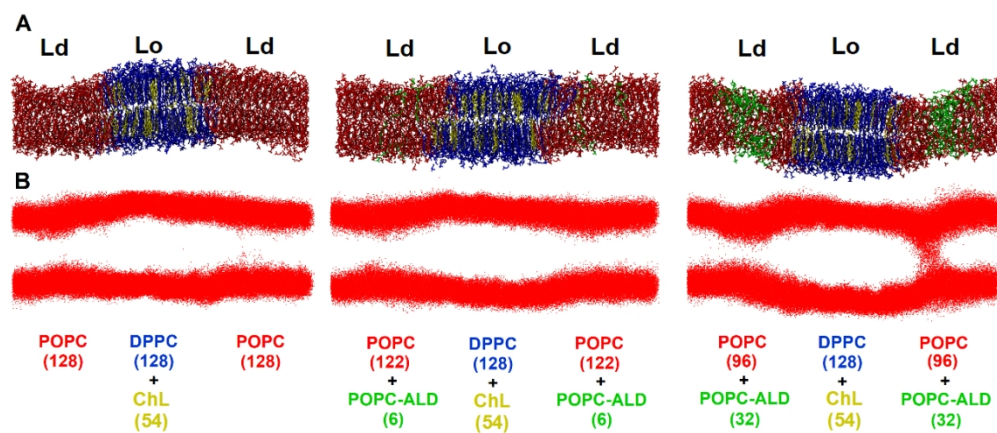


Figure 2. Structure of each lipid and cholesterol (ChL) used in our simulations. See text for the full names.

195x146mm (300 x 300 DPI)



21 Figure 3. (A) Snapshots of heterogeneous membranes at 300 ns of simulation, where the Ld phase is
22 composed of POPC lipid molecules. (B) Trajectories of water molecules. Lipid molecules were removed for
23 clarity and water molecules are represented as red points. All frames of the last 100 ns were overlaid in
24 order to highlight the permeation path of water molecules.

25 343x148mm (96 x 96 DPI)

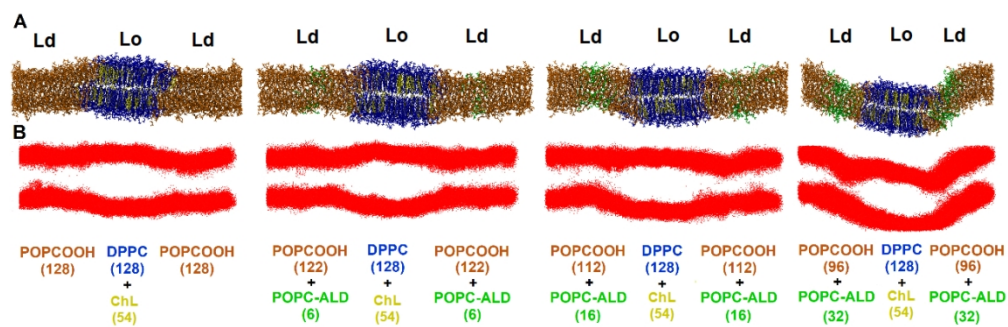


Figure 4. (A) Snapshots of heterogeneous membranes at 300 ns of simulation, where the Ld phase is composed of POPCOOH lipid molecules. (B) Trajectories of water molecules. Lipid molecules were removed for clarity and water molecules are represented as red points. All frames of the last 100 ns were overlaid in order to highlight the permeation path of water molecules.

343x111mm (96 x 96 DPI)

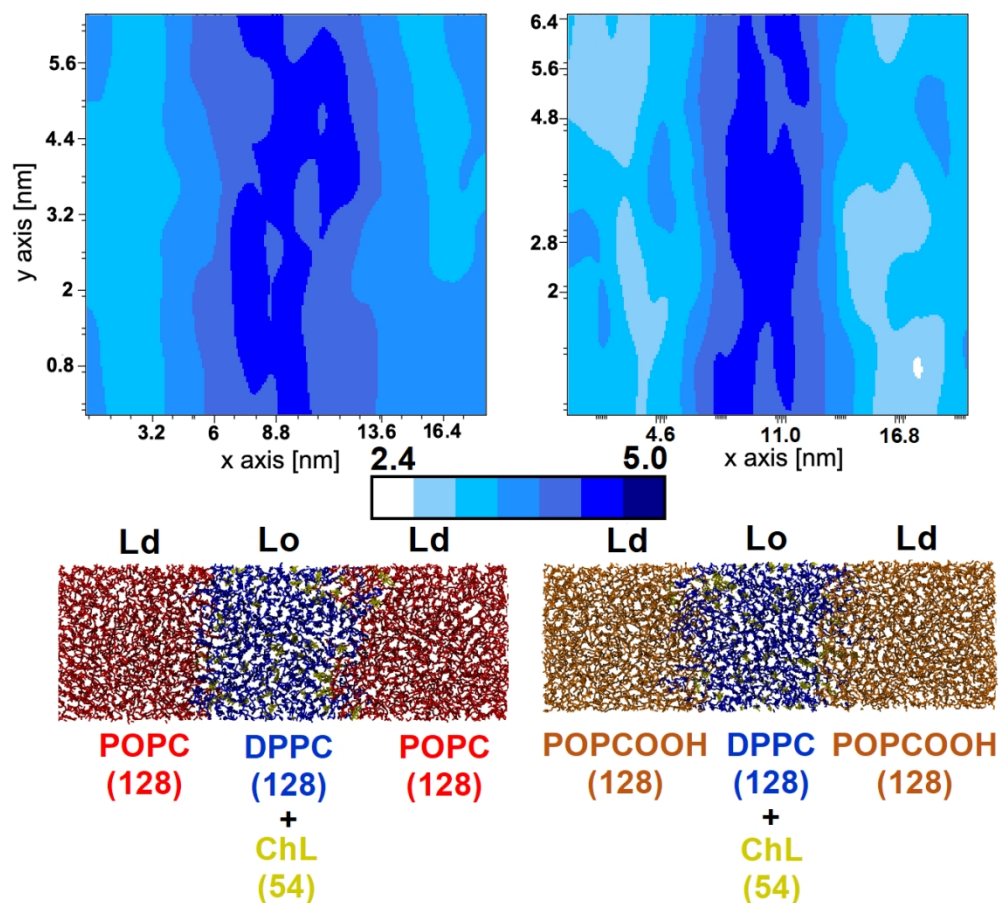


Figure 5. Two-dimensional frame-averaged distribution of the bilayer thickness calculated from the last 100 ns of simulation. The mesh resolution is 40401 and corresponding bin values are equal to 200. These distributions were calculated using the software SuAVE. Both panels represent a top view of the membrane systems. In the upper panel we can see the bilayer thickness of the bottom panel. Box sizes in x and y-axes are the same in upper and bottom figures, but they are represented in different scales.

353x320mm (96 x 96 DPI)

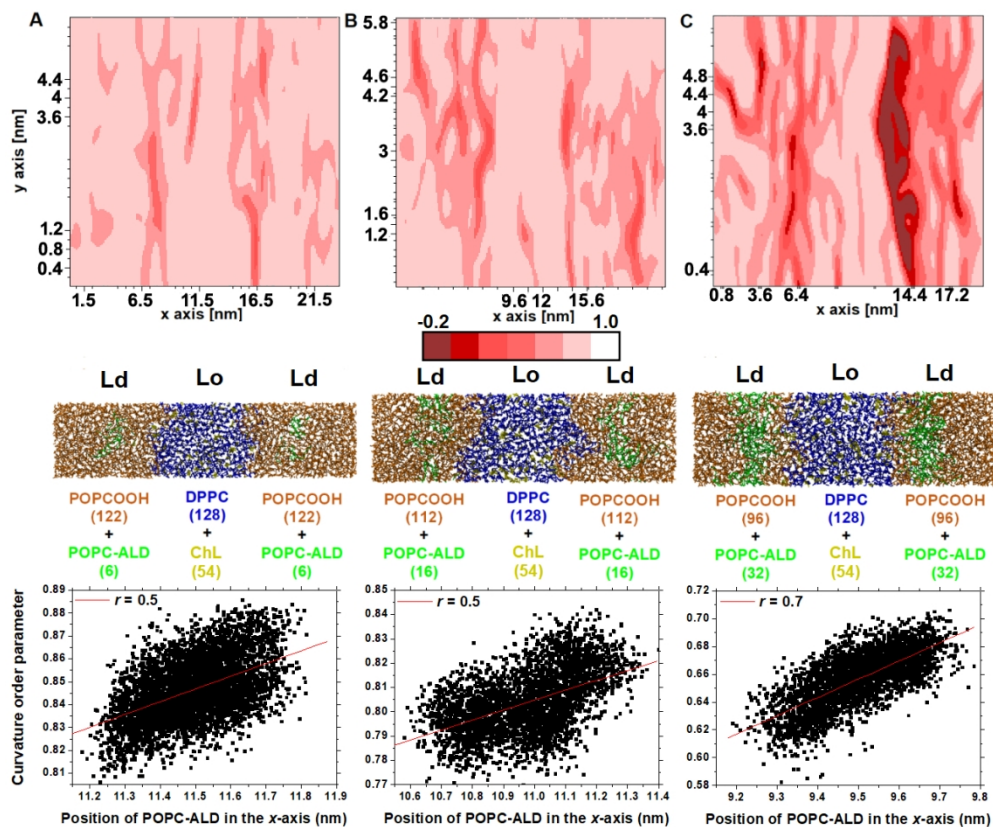


Figure 6. Two-dimensional frame-averaged distribution of the curvature order parameter calculated from the last 100 ns of simulation, for the different systems. These distributions were calculated using the software SuAVE. Both panels represent a top view of the membrane systems. In the upper panel we can see the membrane curvature of the bottom panel. It should be noted that the upper graphs and bottom snapshots are not in the same scale. The bottom-most graphs represent the Pearson correlation coefficient (r) of the curvature order parameter vs position of POPC-ALD lipids.

351x288mm (96 x 96 DPI)

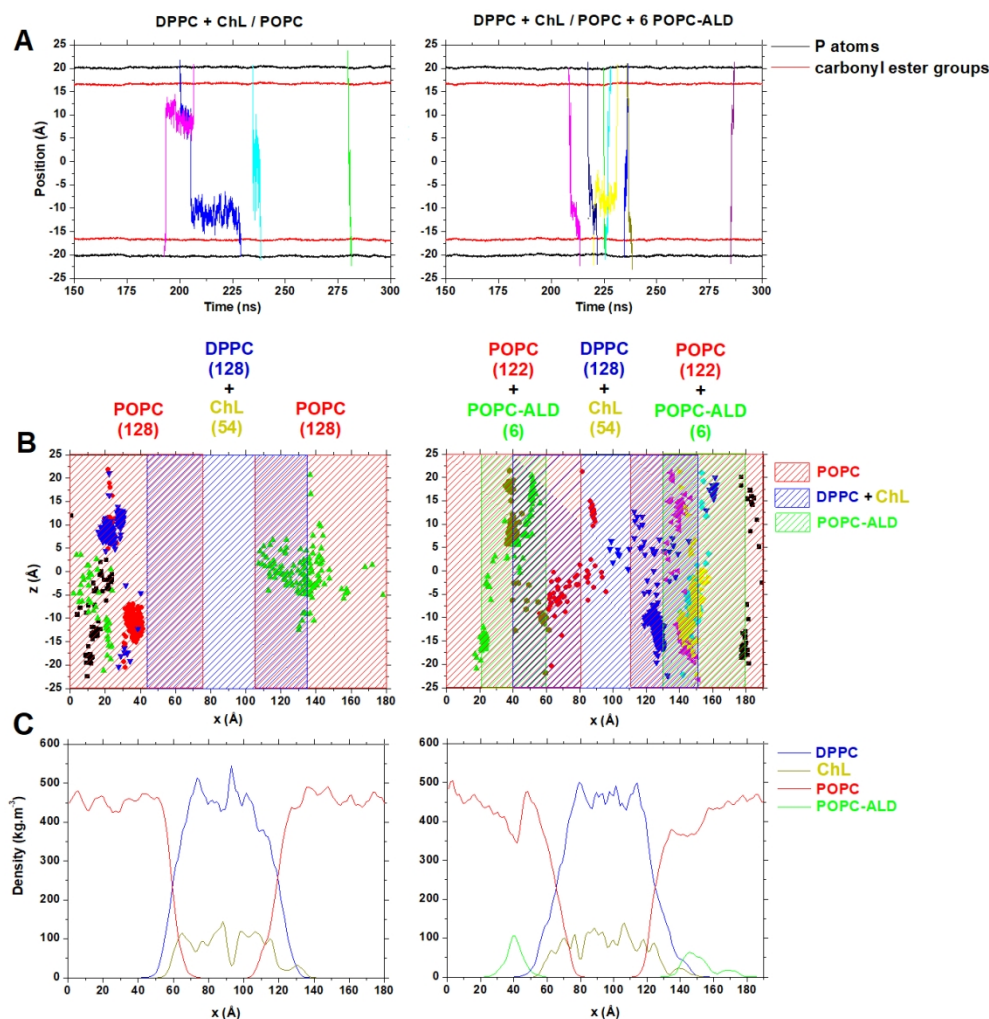


Figure 7. (A) Number of water permeation events calculated from the last 150 ns of simulation to measure the effect caused by addition of POPC-ALD lipid molecules at POPC domains. Each line color represents only one permeation event. (B) Two-dimensional distribution of water permeation events over the last 150 ns of simulation. Each symbol with specific color represents only one permeation event. (C) Density profile along the x-axis calculated from the last 150 ns of simulation.

370x378mm (96 x 96 DPI)

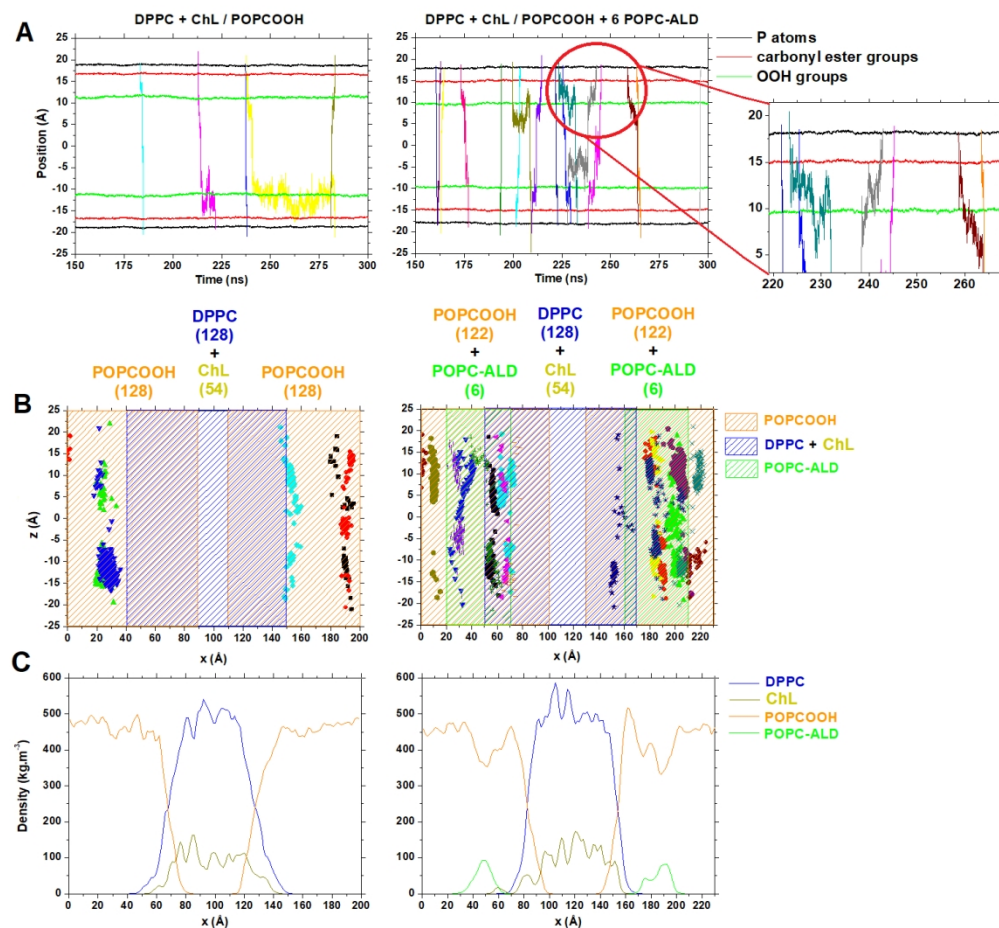


Figure 8. (A) Number of water permeation events calculated from the last 150 ns of simulation to measure the effect caused by addition of POPC-ALD lipid molecules at POPCOOH domains. Each line color represents only one permeation event. Some regions of the graphic on the right side were expanded, in order to show the propensity of the water molecules to spend time at the $-OOH$ groups region. (B) Two-dimensional distribution of water permeation events over the last 150 ns of simulation. Each symbol with specific color represents only one permeation event. (C) Density profile at x-axis calculated from the last 150 ns of simulation.

400x373mm (96 x 96 DPI)

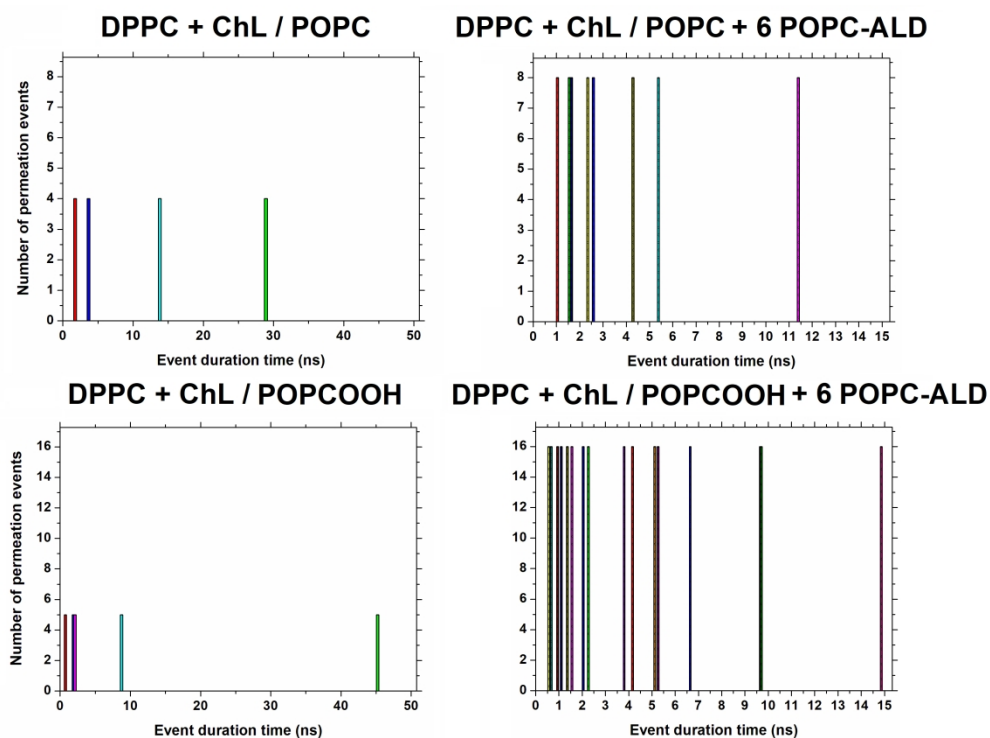


Figure 9. Quantification of the permeation time for the model membranes. Each color bar indicates a duration time of a permeation event. These events were calculated from the last 150 ns of simulation.

868x643mm (96 x 96 DPI)